Open and Hidden Heavy Flavor Production in pp, pA and AA Collisions

R. Vogt

Lawrence Livermore National Laboratory, Livermore, CA 94551, USA
Physics Department, University of California, Davis, CA 95616, USA

Introducing the Cast

Open Charm and Bottom Hadrons

$C_{\rm had}$	**Mass (GeV)**	$c\tau$ **(μm)**	$B(C_{\rm had} \to lX)$ **(%)**	$B(C_{\rm had} \to$ Hadrons**)** **(%)**
$D^+(c\overline{d})$	**1.869**	**315**	**17.2**	$K^-\pi^+\pi^+$ **(9.1)**
$D^-(\overline{c}d)$	**1.869**	**315**	**17.2**	$K^+\pi^-\pi^-$ **(9.1)**
$D^0(c\overline{u})$	**1.864**	**123.4**	**6.87**	$K^-\pi^+$ **(3.8)**
$\overline{D^0}(\overline{c}u)$	**1.864**	**123.4**	**6.87**	$K^+\pi^-$ **(3.8)**
$D^{*\pm}$	**2.010**			$D^0\pi^\pm$ **(67.7)**, $D^\pm\pi^0$ **(30.7)**
D^{*0}	**2.007**			$D^0\pi^0$ **(61.9)**
$D_s^+(c\overline{s})$	**1.969**	**147**	**8**	$K^+K^-\pi^+$ **(4.4)**, $\pi^+\pi^+\pi^-$ **(1.01)**
$D_s^-(\overline{c}s)$	**1.969**	**147**	**8**	$K^+K^-\pi^-$ **(4.4)**, $\pi^+\pi^-\pi^-$ **(1.01)**
$\Lambda_c^+(udc)$	**2.285**	**59.9**	**4.5**	ΛX **(35)**, $pK^-\pi^+$ **(2.8)**
$\Sigma_c^{++}(uuc)$	**2.452**			$\Lambda_c^+\pi^+$ **(100)**
$\Sigma_c^+(udc)$	**2.451**			$\Lambda_c^+\pi^0$ **(100)**
$\Sigma_c^0(ddc)$	**2.452**			$\Lambda_c^+\pi^-$ **(100)**
$B_{\rm had}$	**Mass (GeV)**	$c\tau$ **(μm)**	$B(B_{\rm had} \to lX)$ **(%)**	$B(B_{\rm had} \to$ Hadrons**)** **(%)**
$B^+(u\overline{b})$	**5.2790**	**501**	**10.2**	$\overline{D}^0\pi^-\pi^+\pi^+$ **(1.1)**, $J/\psi K^+$ **(0.1)**
$B^-(\overline{u}b)$	**5.2790**	**501**	**10.2**	$D^0\pi^+\pi^-\pi^-$ **(1.1)**, $J/\psi K^-$ **(0.1)**
$B^0(d\overline{b})$	**5.2794**	**460**	**10.5**	$D^-\pi^+$ **(0.276)**, $J/\psi K^+\pi^-$ **(0.0325)**
$\overline{B^0}(\overline{d}b)$	**5.2794**	**460**	**10.5**	$D^+\pi^-$ **(0.276)**, $J/\psi K^-\pi^+$ **(0.0325)**
$B_c^+(c\overline{b})$	**6.4**			$J/\psi\pi^+$ **(0.0082)**
$B_c^-(\overline{c}b)$	**6.4**			$J/\psi\pi^-$ **(0.0082)**
$\Lambda_b^0(udb)$	**5.624**	**368**		$J/\psi\Lambda$ **(0.047)**, $\Lambda_c^+\pi^-$ **(seen)**

Table 1: Some ground state charm and bottom hadrons with their mass, decay length (when given), branching ratios to leptons (when applicable) and some selected decays to hadrons.

Quarkonium States

Feed down important to total J/ψ and $\Upsilon(1S)$ production

Spectroscopy of quarkonium states described by potential models

$$V(r) = -\frac{\alpha_s}{r} + \sigma r$$

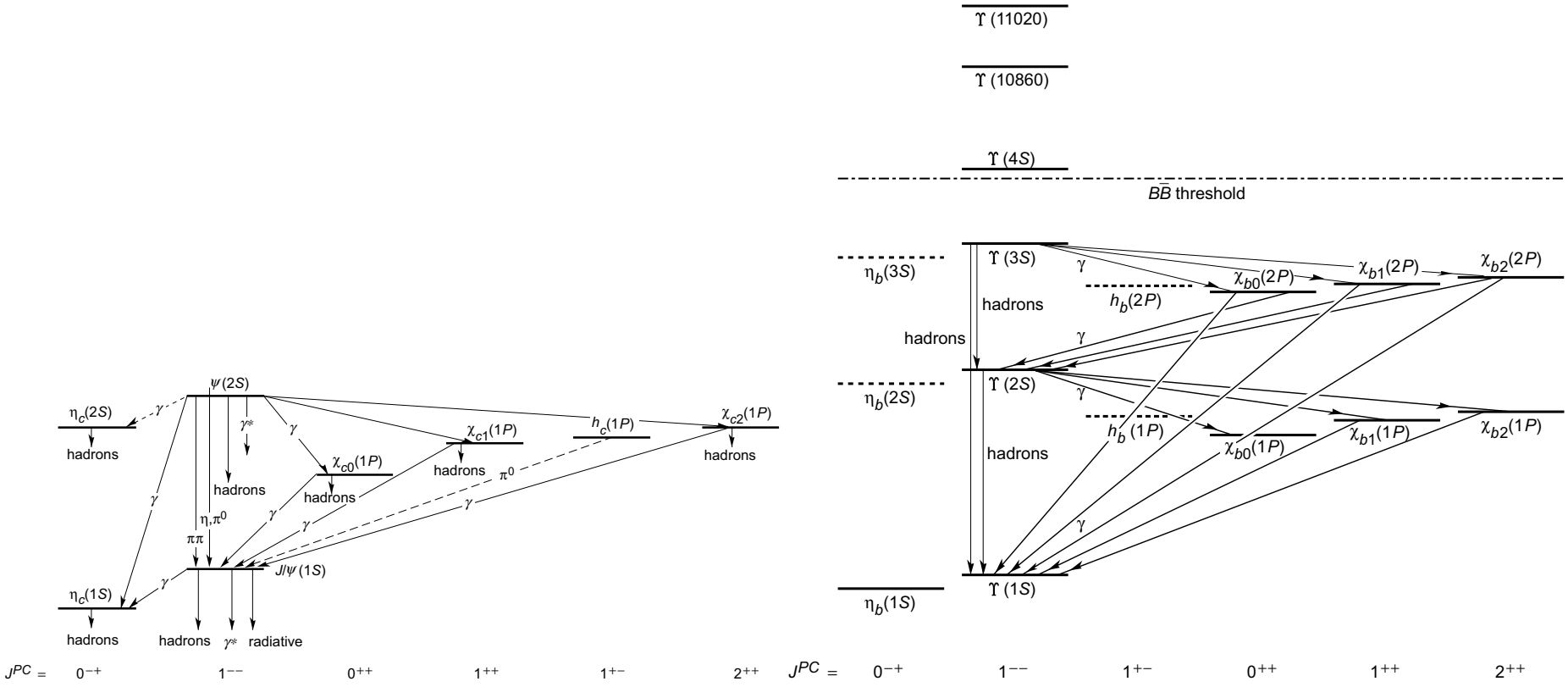

Figure 1: (Left) Charmonium states below the $D\overline{D}$ threshold. (Right) Bottomonium states.

J/ψ vs. Υ – OR – Charm vs. Bottom

Larger b quark masses means that the pQCD expansion is more likely to converge

Heavy quark effective theories work better for heavier flavors

Larger scale means reduced shadowing due to larger x at the same $\sqrt{s}$ as well as higher scale (evolution effects)

$m \gg T$ so no thermal production likely

Lower chance of recombination effects due to smaller production cross sections

Experimental point at LHC: CMS and ATLAS have large magnetic fields so that while J/ψ and ψ' are measured only at relatively high p_T, the Υ states can be measured down to $p_T = 0$, even at midrapidity

J/ψ and ψ' have contributions from B decays that increase at high p_T and so have a prompt (direct J/ψ and ψ', feed down from higher states for the J/ψ) and a non-prompt (B decay) component

Production in pp Collisions

Open Heavy Flavor

- **Fixed-Order Total Cross Sections**
- **Fixed-Order Next-to-Leading Logarithm (FONLL) Approach**
- **Next-to-Leading Order Inclusive/Exclusive Production (HVQMNR)**
- **POWHEG-hvq**
- **Leading Order Event Generators**
- **k_T-Factorization Approach**

Calculating Heavy Flavors in Perturbative QCD

'Hard' processes have a large scale in the calculation that makes perturbative QCD applicable, since $m \neq 0$, heavy quark production is a 'hard' process

All production models essentially follow the same procedure for collinear factorization, some modification for k_T-factorization or saturation

Production cross section in a pp collision

$$\sigma_{pp}(S, m^2) = \sum_{i,j=q,\overline{q},g} \int_{4m_Q^2/S}^1 \frac{d\tau}{\tau} \int dx_1\, dx_2\, \delta(x_1 x_2 - \tau) f_i^p(x_1, \mu_F^2)\, f_j^p(x_2, \mu_F^2)\, \widehat{\sigma}_{ij}(s, m^2, \mu_F^2, \mu_R^2)$$

f_i^A are nonperturbative parton distributions, determined from global fits, x_1, x_2 are proton momentum fractions carried by partons i and j, $\tau = s/S$

$\widehat{\sigma}_{ij}(s, m^2, \mu_F^2, \mu_R^2)$ is hard partonic cross section calculable in QCD in powers of α_s^{2+n}: leading order (LO), $n = 0$; next-to-leading order (NLO), $n = 1$ ...

Number of light flavors in α_s based on mass scale: $n_{\rm lf} = 3$ for c and 4 for b for NLO-based calculations, $n_{\rm lf} = 4$ for c and 5 for b for FONLL

Results depend strongly on quark mass, m, factorization scale, μ_F, in the parton densities and renormalization scale, μ_R, in α_s

Defining Theoretical Uncertainty

Fiducial uncertainty obtained from region of mass and scale that should encompass the true value (FONLL)

- **For** $\mu_F = \mu_R = m$**, vary mass,** $1.3 < m_c < 1.7$**,** $4.5 < m_b < 5.0$ **GeV;**
- **For** $m_c = 1.5$ **and** $m_b = 4.75$ **GeV, vary scales independently within a factor of two:** $(\mu_F/m, \mu_R/m) = (1,1)$**, (2,2), (0.5,0.5), (0.5,1), (1,0.5), (1,2), (2,1).**

Fitting the total heavy flavor cross sections

- **Take lattice value for** m_c **and** $1S$ **value for** m_b**, 1.27 and 4.65 GeV respectively with** 3σ **mass uncertainty**
- **Vary scales independently within** 1σ **of fitted region:** $(\mu_F/m, \mu_R/m) = (C,C)$**, (H,H), (L,L), (H,C), (C,H), (L,C), (C,L)**

The uncertainty band in all cases comes from the upper and lower limits of mass and scale uncertainties added in quadrature

The resulting theoretical uncertainties can be large, especially for charm; good for containing full uncertainty range but less so for comparing to high statistics data

Pinning Down Open Charm Uncertainties by Fitting $\sigma_{c\overline{c}}$

Caveat: full NNLO cross section unknown, could still be large corrections

Employ $m = 1.27$ GeV, lattice value at $m(3\,\mathrm{GeV})$

Use subset of $c\overline{c}$ total cross section data to fix best fit values of μ_F/m and μ_R/m

Result with $\Delta\chi^2 = 1$ gives uncertainty on scale parameters; $\Delta\chi^2 = 2.3$ gives one standard deviation on total cross section

LHC results from ALICE agrees well even though not included in the fits

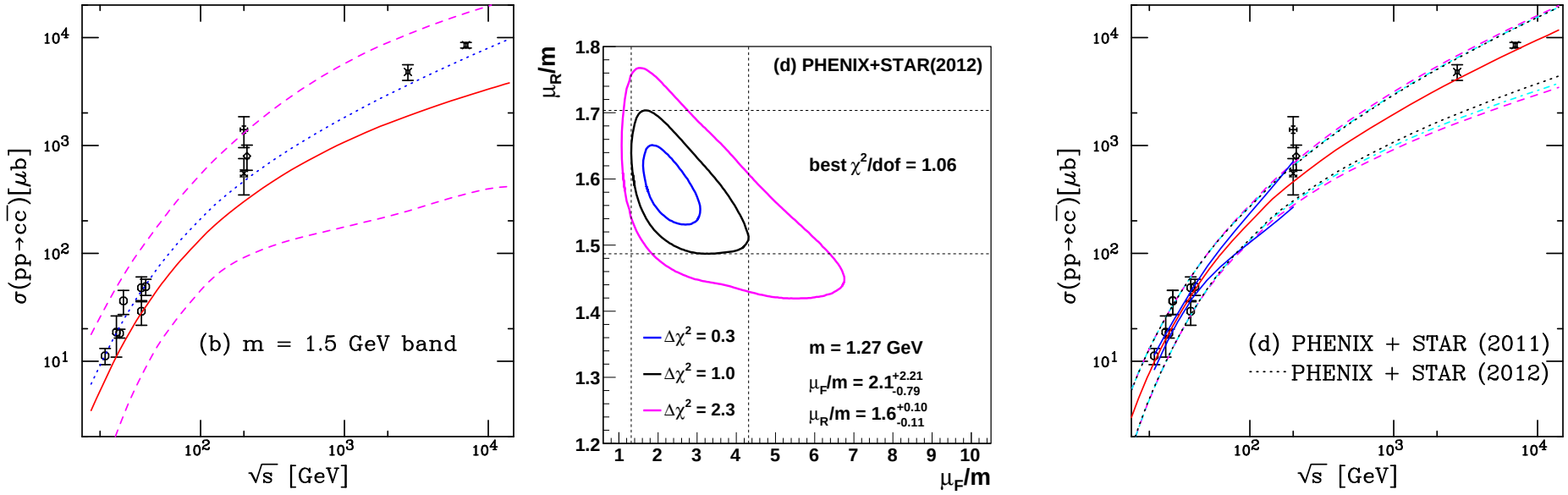

Figure 2: (Left) Total charm cross section uncertainty using FONLL fiducial parameters compared to a calculation with $m = 1.2$ GeV, $mu_F/m = mu_R/m = 2$. (Center) The χ^2/dof contours for fits including the STAR 2011 cross section but excluding the STAR 2004 cross section. The best fit values are given for the furthest extent of the $\Delta\chi^2 = 1$ contours. (Right) The energy dependence of the charm total cross section compared to data. The best fit values are given for the furthest extent of the $\Delta\chi^2 = 1$ contours. The central value of the fit in each case is given by the solid red curve while the dashed magenta curves and dot-dashed cyan curves show the extent of the corresponding uncertainty bands. The dashed curves outline the most extreme limits of the band. In addition, the dotted black curves show the uncertainty bands obtained with the 2012 STAR results while the solid blue curves in the range $19.4 \leq \sqrt{s} \leq 200$ GeV represent the uncertainty obtained from the extent of the $\Delta\chi^2 = 2.3$ contour. [R. Nelson, RV, and A.D. Frawley, PRC **87** (2013) 014908.]

Inclusive Production with FONLL

Single inclusive calculation of heavy flavor: quark; hadron; and semileptonic decay distributions – most relevant for $p_T >> m$ where p_T is dominant scale

Kinematics of only one heavy quark kept, the other is integrated away

Generates p_T, y grid of heavy quark cross section, calculated in pQCD

Fragmentation of heavy quarks, Q, into heavy-flavor hadrons, H_Q, described by fragmentation functions appropriate to FONLL approach, $D(Q \to H_Q)$, extracted from e^+e^- annihilation data

Includes resummed terms (RS) of order $\alpha_s^2(\alpha_s \log(p_T/m))^k$ (leading log – LL) and $\alpha_s^3(\alpha_s \log(p_T/m))^k$ (NLL); subtracts fixed-order (FO) terms, retaining only logarithmic mass dependence ("massless" limit of FO calculation (FOM0)), obtained in the same renormalization scheme

$G(m, p_T) \sim p_T^2/(p_T^2 + cm^2)$ interpolates between FO and RS for same number of light flavors (Cacciari and Nason)

$$\mathrm{FONLL} = \mathrm{FO} + (\mathrm{RS} - \mathrm{FOM0})G(m, p_T)$$

Smaller cross section than FO calculation since heavy flavor treated as a light degree of freedom ($n_{\mathrm{lf}} = 4$ for charm) so that $\alpha_s(\mu_R)$ smaller than in production calculation with $n_{\mathrm{lf}} = 3$ for charm

Results on LHC Heavy Flavor Distributions

All calculations with FONLL: excellent agreement with $\sqrt{s} = 7$ TeV ALICE pp data on muons in the forward region $(2.5 < y < 4)$

Leptons from semi-leptonic heavy flavor decays include contributions from $D \to \mu X$, $B \to \mu X$, $B \to D \to \mu X$, all with $\sim 10\%$ decay branching ratios

Exchanging fit results with results based on $m = 1.5$ GeV gives narrower uncertainty without reducing agreement with data

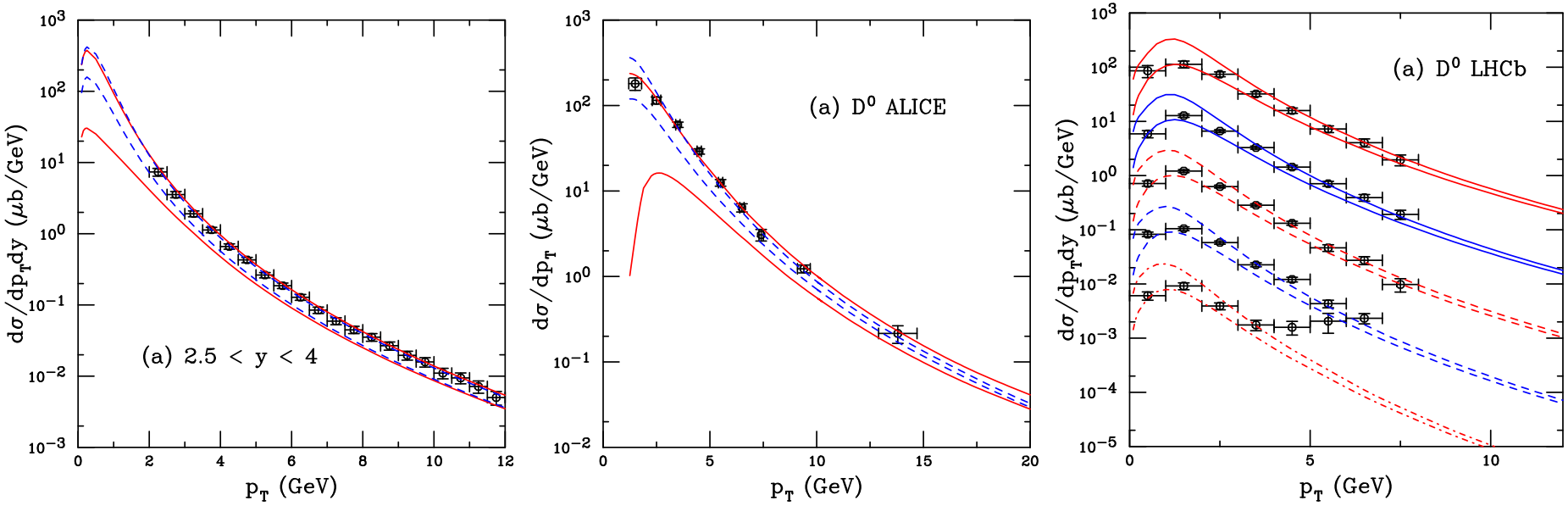

Figure 3: (Left) Comparison of the single lepton p_T distributions in the rapidity interval $2.5 < y < 4$ at $\sqrt{s} = 7$ TeV calculated with the FONLL set for charm (solid red) and the fitted set with $m = 1.27$ GeV (dashed black). (Center) Our calculations are compared with the reconstructed ALICE D^0 data in $|y| \leq 0.5$. The FONLL uncertainty bands with the fiducial charm parameter set are shown by the red solid curves while the blue dashed curves are calculated with the charm fit parameters. (Right) Our calculations are compared with the reconstructed LHCb D^0 data in the rapidity intervals: $2 < y < 2.5$ (solid red); $2.5 < y < 3$ (solid blue); $3 < y < 3.5$ (dashed red); $3.5 < y < 4$ (dashed blue); and $4 < y < 4.5$ (dot-dashed red). The rapidity intervals are separated by a factor of 10 to facilitate comparison. The lowest rapidity interval, $2 < y < 2.5$, is not scaled. [R. Nelson, RV, and A.D. Frawley, PRC **87** (2013) 014908.]

Fixed Order Exclusive Calculations

HVQMNR (Mangano, Nason and Ridolfi): exclusive NLO heavy flavor calculation, no resummed terms but is a reasonable description of p_T distributions when p_T is not too high (quark distributions very similar to FONLL, difference is in fragmentation functions)

Generates 1-D distributions of inclusive (single quark p_T and y) and exclusive ($Q\overline{Q}$ pair p_T, y, M, ϕ) observables, not really possible to obtain event list with correct weights

Default fragmentation function is Peterson function; can be turned off

Negative weight MC; incomplete cancellation of divergences, no leading log resummation

POWHEG-hvq (Frixione, Nason and Ridolfi): heavy flavor hard event generator, exclusive calculation with NLO matrix elements added correctly

Positive weight MC, includes leading log resummation

Can be run either standalone to obtain NLO events or interfaced to shower Monte Carlos like HERWIG and PYTHIA

FONLL vs. HVQMNR c and b

Charm distributions very similar up to $p_T \sim 10$ GeV, for $p_T/m > 8$, the $\log(p_T/m)$ terms that are not resummed in HVQMNR change p_T slope relative to FONLL

Bottom distributions almost identical up to $p_T \sim 50$ GeV, since m is bigger, the log problem gets pushed to higher p_T

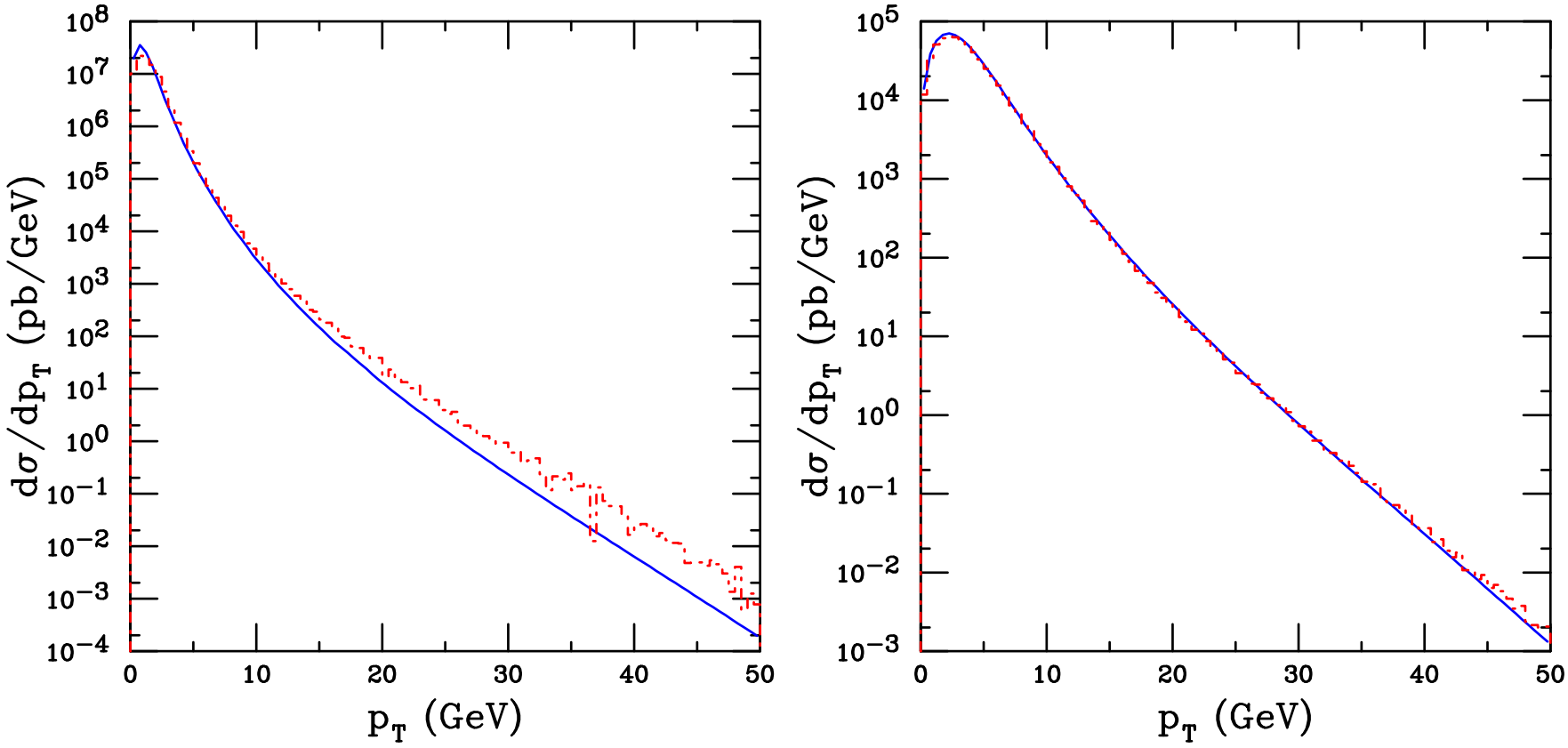

Figure 4: The p_T distributions calculated using FONLL (blue solid) are compared to HVQMNR (red histogram) up to high p_T. The charm (left) and bottom (right) quark distributions are compared at $\sqrt{s} = 200$ GeV for $0 < y < 0.5$.

FONLL vs. POWHEG+PYTHIA D^0 and B^0

Advantage of POWHEG+PYTHIA is that it serves as an event generator as well as simulating multiple gluon radiation from external legs

Both methods allow for hadronization of heavy flavor mesons as well as semileptonic decays

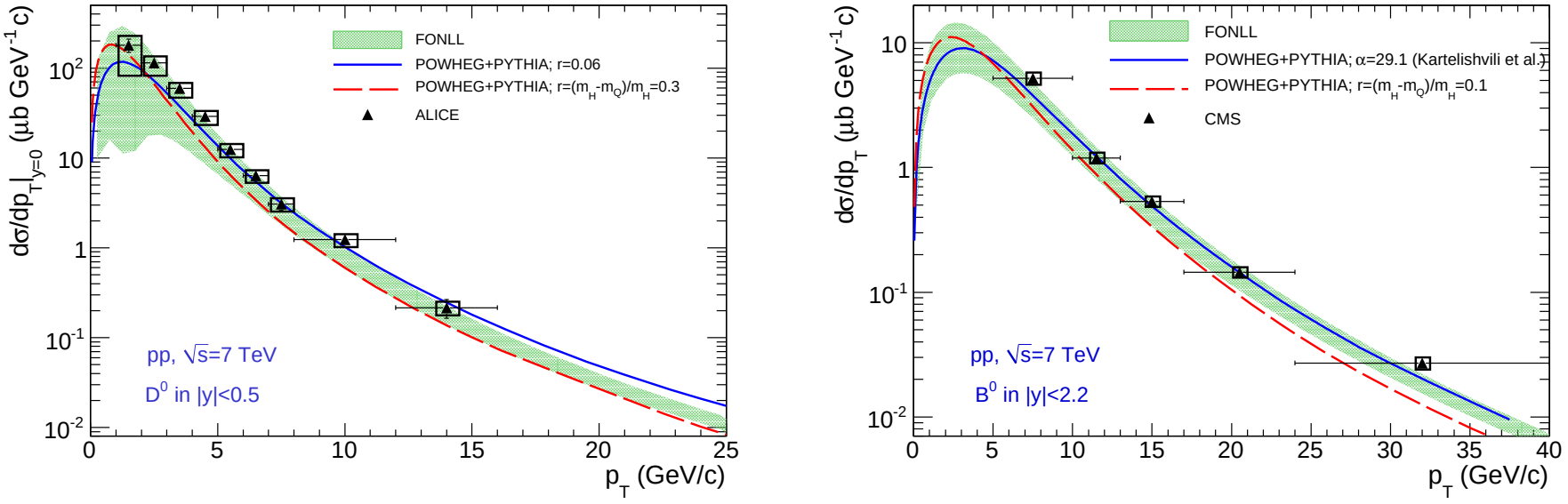

Figure 5: POWHEG+PYTHIA predictions for D^0 production with $m_c = 1.3$ GeV in ALICE (left) and B^0 production with $m_b = 4.8$ GeV in CMS (right). The calculations employ two different fragmentation parameters. The results are compared to the FONLL uncertainty bands. [W. M. Alberico *et al*, arXiv:1305.7421.]

PYTHIA

PYTHIA uses leading order matrix elements

To simulate next-to-leading order cross section, PYTHIA requires separate calculations depending on how many heavy quarks are at a hard vertex: pair creation (2), flavor excitation (1) and gluon splitting (0) rather than grouping diagrams by initial state as in NLO ($q\overline{q}$, gg, qg)

Splitting and excitation are sub-classes of gg and qg NLO diagrams

PYTHIA typically gives larger cross sections than NLO because no interference terms, *e.g.* different gg terms added separately

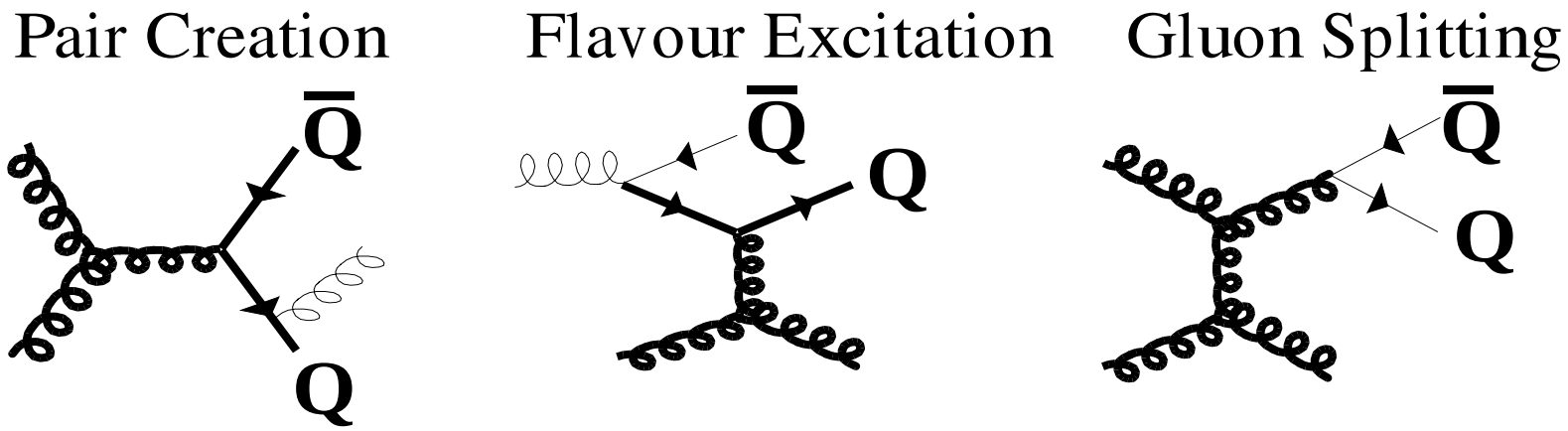

Figure 6: Examples of pair creation, flavor excitation and gluon splitting. The thick lines correspond to the hard process, the thin ones to the parton shower.

HIJING $B\overline{B}$

Uses PYTHIA matrix elements for hard processes

Allows for multiple overlapping flux tubes leading to strong longitudinal color field (SCF) effects

SCF effects modeled by varying κ and momentum cutoff with $\sqrt{s}$ and A, use larger κ for strangeness and charm production

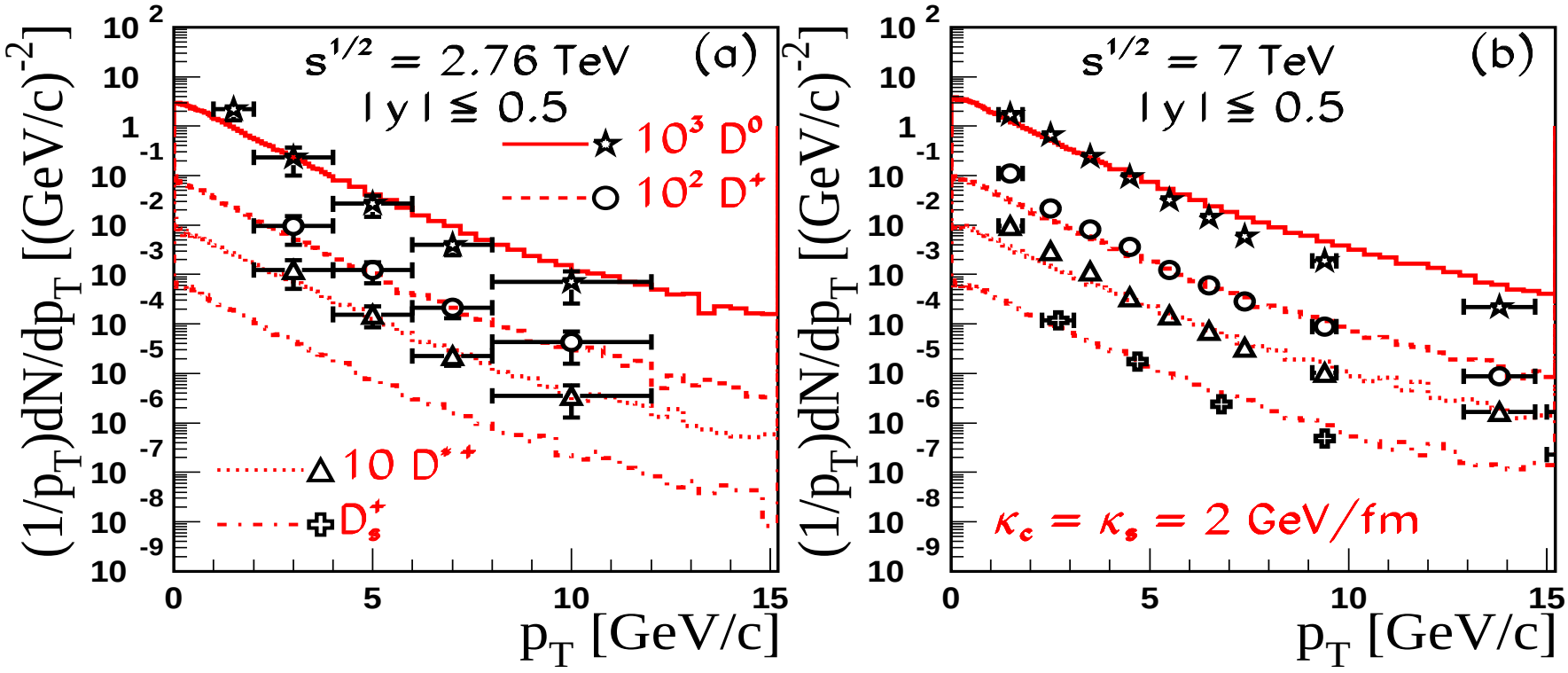

Figure 7: HIJING $B\overline{B}$ calculations for, from top to bottom, D^0, D^+, D^* and D_s^+ production in pp collisions at $\sqrt{s} = 2.76$ and 7 TeV. [V. Topor Pop *et al.*, arXiv:1306.0885.]

k_T Factorization

Uses off-shell leading order matrix elements for $g^*g^* \to c\overline{c}$ (Collins and Ellis) together with unintegrated gluon distributions (UGD) that depend on the gluon transverse momenta as well as the usual dependence on x and factorization scale μ_F

Calculation of D meson and $D\overline{D}$ pair production by Maciula and Szczurek at $\sqrt{s} = 7$ TeV in pp collisions compares results for several UGDs

$$\frac{d\sigma(pp \to c\bar{c}X)}{dy_1 dy_2 d^2p_{1T} d^2p_{2T}} = \frac{1}{16\pi^2 \hat{s}^2} \int \frac{d^2k_{1T}}{\pi} \frac{d^2k_{2T}}{\pi} \overline{|\mathcal{M}_{g^*g^* \to c\,\bar{c}}|^2} \delta^2\left(\vec{k}_{1T} + \vec{k}_{2T} - \vec{p}_{1T} - \vec{p}_{2T}\right) \mathcal{F}_g(x_1, k_{1T}^2, \mu_F^2) \mathcal{F}_g(x_2, k_{2T}^2, \mu_F^2)$$

$$\frac{d\sigma(pp \to D\bar{D}X)}{dy_1 dy_2 d^2p_{1T}^D d^2p_{2T}^{\bar{D}}} \approx \int \frac{D_{c\to D}(z_1)}{z_1} \cdot \frac{D_{\bar{c}\to \bar{D}}(z_2)}{z_2} \cdot \frac{d\sigma(pp \to c\bar{c}X)}{dy_1 dy_2 d^2p_{1T}^c d^2p_{2T}^{\bar{c}}} dz_1 dz_2 \,, \tag{1}$$

Fragmentation included for heavy quark hadronization, results suggest that smaller value of ϵ (Peterson function parameter) gives better agreement with data

Unintegrated Gluon Distributions

UGDs depend on LO k_T-integrated parton densities and Sudakov form factor, T_g, function of parton splitting functions and phase space restriction $\Delta = k_T/(k_T+\mu_F)$

$$\mathcal{F}_g^{\rm KMR}(x,k_T^2,\mu_F^2) = f_g(x,k_T^2,\mu_F^2) = T_g(k_T^2,\mu_F^2)\,\frac{\alpha_s(k_T^2)}{2\pi}\sum_{b=g,q}\int_x^1 dz\,P_{gb}(z)\,b\left(\frac{x}{z},k_T^2\right)$$

$$T_g(k_T^2,\mu_F^2) = \exp\left(-\int_{k_T^2}^{\mu_F^2}\frac{d\kappa_T^2}{\kappa_T^2}\,\frac{\alpha_s(\kappa_T^2)}{2\pi}\left(\int_0^{1-\Delta}dz\;z\,P_{gg}(z)+n_F\int_0^1 dz\,P_{qg}(z)\right)\right)$$

$$\mathcal{F}_g^{\rm other}(x,k_T^2,\mu_F^2) = \frac{1}{k_T^2}f_g(x,k_T^2,\mu_F^2) = \frac{T_g(k_T^2,\mu_F^2)}{k_T^2}\frac{\alpha_S(k_T^2)}{2\pi}\times$$
$$\int_x^1 dz\left[\sum_q P_{gq}(z)\frac{x}{z}q\left(\frac{x}{z},k_T^2\right)+P_{gg}(z)\frac{x}{z}g\left(\frac{x}{z},k_T^2\right)\Theta\left(\frac{\mu_F}{\mu_F+k_T}-z\right)\right]$$

Normalization condition $g(x,\mu_F^2) = \int_0^{\mu^2} dk_T^2\, f_g(x,k_T^2,\mu_F^2)$

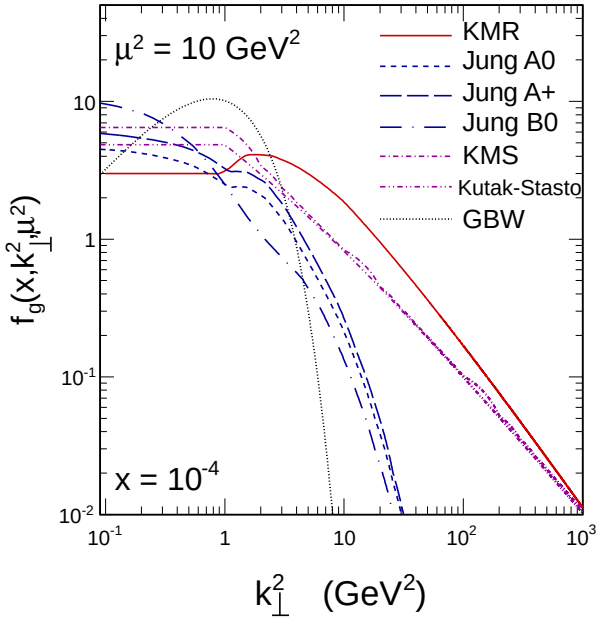

Figure 8: Comparison of UGDs as a function of k_T^2 for fixed x. [Maciula and Szczurek, arXiv:1301.3033.]

k_T Factorization Enhances Low p_T Region

Difference between KMR UGDs and FONLL only at $p_T < 5$ GeV

Changing LO k_T-integrated parton densities, scale choice, charm quark mass and fragmentation parameter does not improve agreement with data for $p_T < 10$ GeV

Similar results for other D mesons and rapidity regions

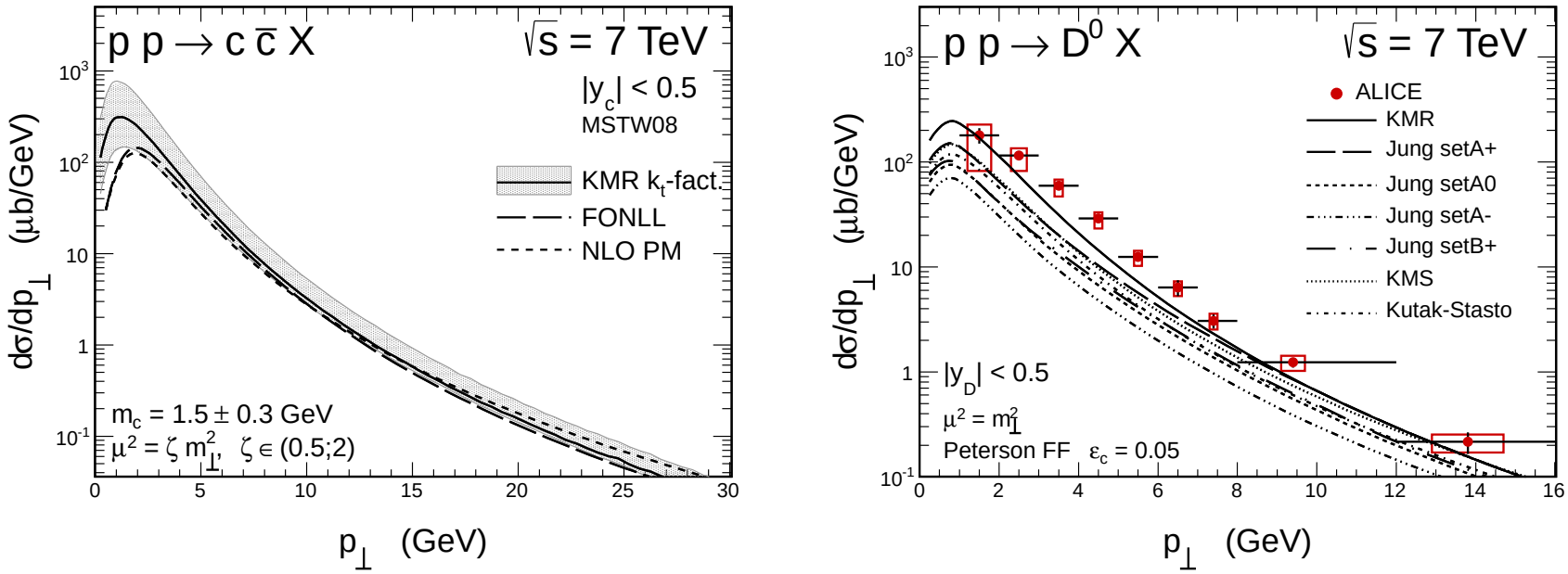

Figure 9: (Left) Comparison of UGDs as a function of k_T^2 for fixed x. (Center) Charm quark uncertainty band calculated with KMR UDG compared to the central FONLL value and MC@NLO (NLO PM) in $|y| < 0.5$ at 7 TeV. (Right) Different UGDs compared to ALICE D^0 data. [Maciula and Szczurek, arXiv:1301.3033.]

Charm Pair Production

Data not compared to NLO collinear factorization

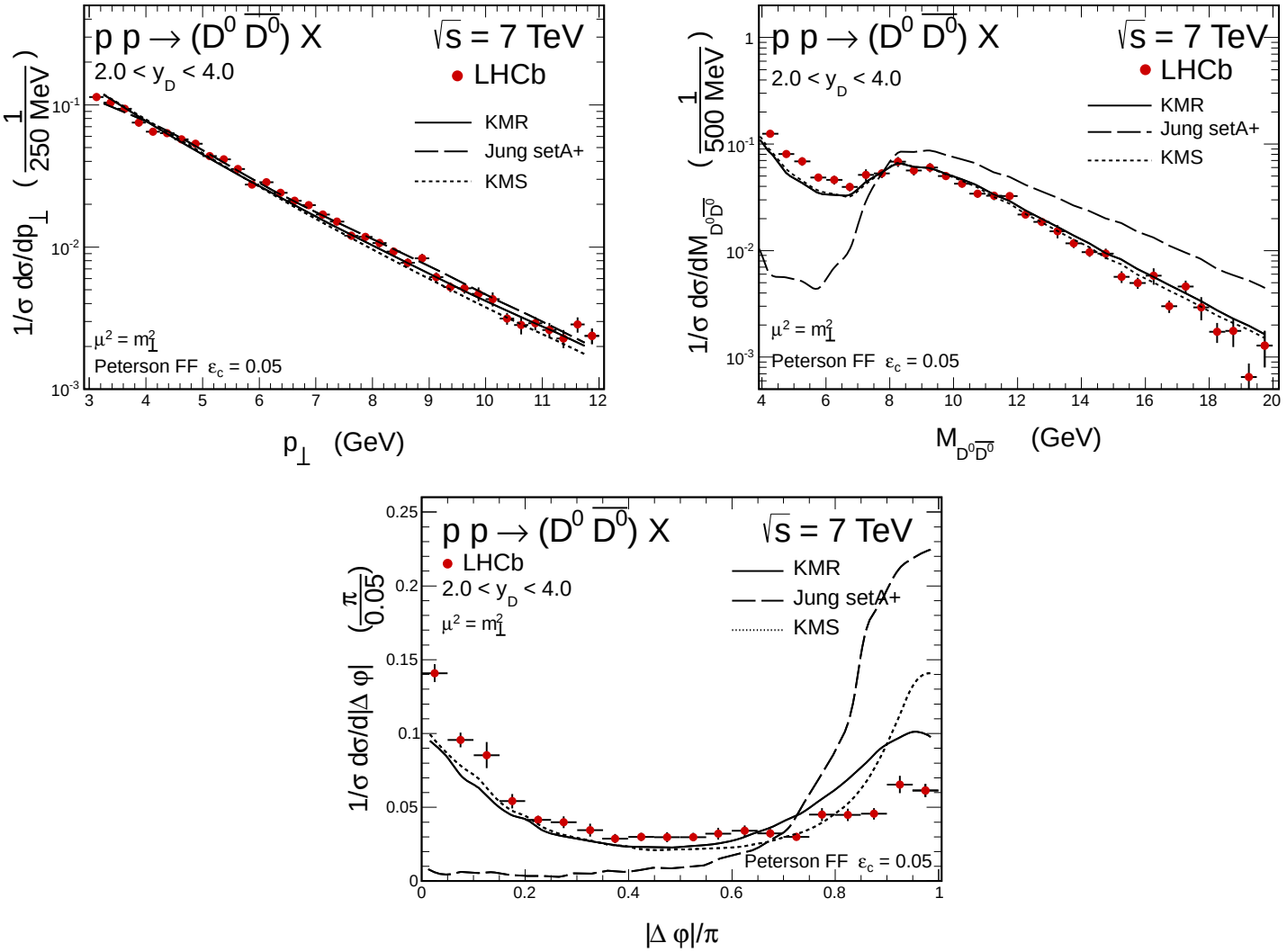

Figure 10: Comparison of $D^0\overline{D}^0$ pair p_T (top left), M (top right) and $|\Delta\phi|/\pi$ (bottom) with data from LHCb. [Maciula and Szczurek, arXiv:1301.3033.]

Hidden Heavy Flavor

- **Color Evaporation Model (CEM)**
- **Color Singlet Model (CSM)**
- **Nonrelativistic QCD (NRQCD) – also known as Color Octet Model (COM)**
- **Global Fits (CSM + COM)**

Color Evaporation Model

All quarkonium states are treated like $Q\overline{Q}$ ($Q = c, b$) below $H\overline{H}$ ($H = D, B$) threshold

Distributions for all quarkonium family members identical. Thus production ratios should also be independent of $\sqrt{S}$, p_T, x_F.

At LO, $gg \to Q\overline{Q}$ and $q\overline{q} \to Q\overline{Q}$; NLO add $gq \to Q\overline{Q}q$

$$\sigma_Q^{\rm CEM} = F_Q \sum_{i,j} \int_{4m_Q^2}^{4m_H^2} d\hat{s} \int dx_1 dx_2 \; f_{i/p}(x_1, \mu^2) \; f_{j/p}(x_2, \mu^2) \; \hat{\sigma}_{ij}(\hat{s}) \; \delta(\hat{s} - x_1 x_2 s)$$

First, values of m_Q and Q^2 for several parton densities fixed from NLO calculation of $Q\overline{Q}$ total cross sections

Inclusive F_Q fixed by comparison of NLO calculation of $\sigma_Q^{\rm CEM}$ to $\sqrt{S}$ dependence of J/ψ and Υ cross sections, $\sigma(x_F > 0)$ and $Bd\sigma/dy|_{y=0}$ for J/ψ, $Bd\sigma/dy|_{y=0}$ for Υ

Data and branching ratios used to separate the F_Q's for each quarkonium state

Resonance	J/ψ	ψ'	χ_{c1}	χ_{c2}	Υ	Υ'	Υ''	$\chi_b(1P)$	$\chi_b(2P)$
$\sigma_i^{\rm dir}/\sigma_H$	**0.62**	**0.14**	**0.6**	**0.99**	**0.52**	**0.33**	**0.20**	**1.08**	**0.84**
f_i	**0.62**	**0.08**	**0.16**	**0.14**	**0.52**	**0.10**	**0.02**	**0.26**	**0.10**

Table 2: The ratios of the direct quarkonium production cross sections, $\sigma_i^{\rm dir}$, to the inclusive J/ψ and Υ cross sections, denoted σ_H, and the feed down contributions of all states to the J/ψ and Υ cross sections, f_i, Digal *et al.*.

J/ψ Cross Sections from $c\bar{c}$ Fits

Take results of $c\bar{c}$ fits, calculate NLO J/ψ cross section in CEM, fit scale factor F_C (needed to match the $c\bar{c}$ cross section below the $D\overline{D}$ threshold to the inclusive J/ψ cross section) with central value of parameter sets – tighter uncertainty band

CEM calculation reproduces shape of J/ψ p_T and y distributions rather well with single parameter

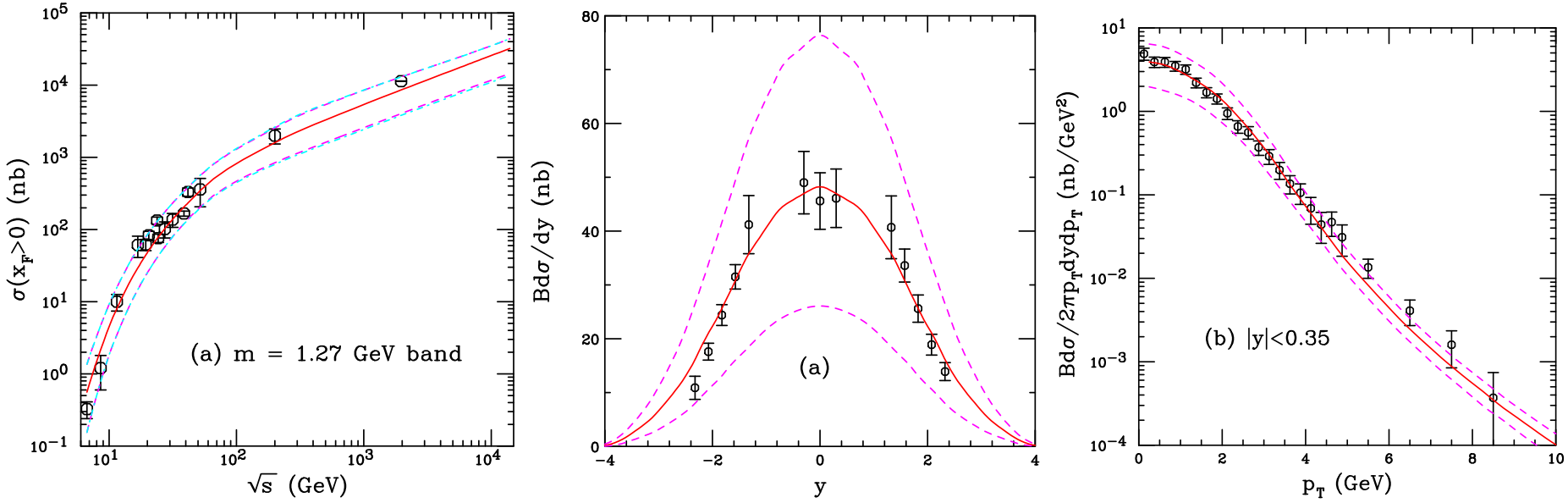

Figure 11: (Left) The uncertainty band on the forward J/ψ cross section. The dashed magenta curves and dot-dashed cyan curves show the extent of the corresponding uncertainty bands. The dashed curves outline the most extreme limits of the band. The J/ψ rapidity distribution (center) and the midrapidity p_T distributions (right) and their uncertainties. The results are compared to PHENIX pp measurements at $\sqrt{s} = 200$ GeV. The solid red curve shows the central value while the dashed magenta curves outline the uncertainty band. A $\langle k_T^2 \rangle$ kick of 1.19 GeV^2 is applied to the p_T distributions. [R. Nelson, RV, and A.D. Frawley, PRC **87** (2013) 014908.]

Color Singlet Model Production

CSM assumes factorization of production process into perturbative production of on-shell Q and $\overline{Q}$ at scale m_T of the final state (assumes that the color and spin of the $Q\overline{Q}$ pair is unchanged by binding)

The heavy quark velocity in the bound state must be small, thus it is assumed to be created with the heavy quarks at rest in the meson frame, the static approximation

Static approximation amounts to considering only first non-zero part of amplitude when the perturbative matrix element $\mathcal{M}$ is expanded in powers of relative $Q\overline{Q}$ momentum p; for S states

$$\int dp\Phi(\vec{p})\mathcal{M}(p)\delta(2p^0) \simeq \mathcal{M}(p=0)\Psi(\vec{x}=0)$$

Coordinate-space wavefunction Ψ is non-perturbative input which can be extracted from leptonic decay width: $|\Psi(0)|^2$ for S states; $|\Psi'(0)|^2$ for P states since $|\Psi(0)| = 0$

At LO, S state production is by $gg \to \psi g$ at $\mathcal{O}(\alpha_s^3)$ while $gg \to \chi_c$, $\mathcal{O}(\alpha_s^2)$, is allowed

Expectation that prompt J/ψ and ψ' production should be small and high p_T J/ψ's should come from χ_c decays

Strong disagreement with CDF production data, higher order CS contributions reduce disagreement with data but with growing uncertainty

Higher Order Corrections Improve CSM Agreement

Higher order contributions to the CSM: complete NLO and a partial NNLO (NNLO*) results bring high p_T ($p_T > 5$ GeV) quarkonium production into better agreement with Tevatron data at $\sqrt{s} = 1.96$ TeV

J/ψ and ψ' still below the data, cleaner ψ' has no feed down contribution (all prompt)

$\Upsilon(1S)$ calculation is prompt data (inclusive, *i.e.* with feed down included) times the direct fraction, essentially assuming that the feed down contribution has the same p_T distribution – similar to CEM

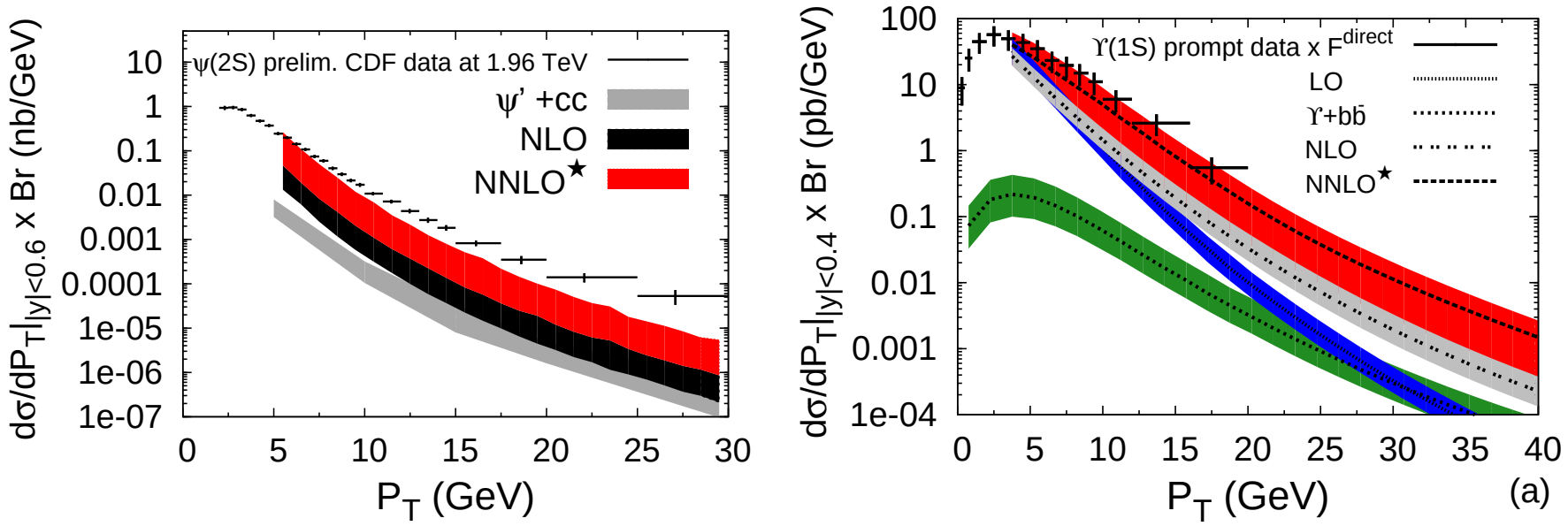

Figure 12: Recent CSM p_T distributions up to NLO and NNLO* compared to (left) ψ' and (right) $\Upsilon(1S)$ measurements by CDF at $\sqrt{s} = 1.96$ TeV. [From QWG report, Eur. Phys. J C **71** (2011) 1534.]

Color Octet (NRQCD) Production

New Fock states introduced to cancel infrared divergences in light hadron decays of χ_{c1} into two gluons, one real and one virtual; when real gluon is soft, decay width diverges without new terms

These new Fock states included $gc\overline{c}(^3S_1)$ color octet and introduced new momentum scale, Λ, for light quark

Based on systematic expansion in strong coupling constant, α_s, and relative velocity of Q and $\overline{Q}$, v (in bound states, $v_c^2 \sim 0.23$ and $v_b^2 \sim 0.08$)

$$|\psi_\mathcal{C}\rangle = \mathcal{O}(1)|Q\overline{Q}[^3S_1^{(1)}]\rangle + \mathcal{O}(v)|Q\overline{Q}[^3P_J^{(8)}]g\rangle + \mathcal{O}(v^2)|Q\overline{Q}[^3S_1^{(1,8)}]gg\rangle + \mathcal{O}(v^2)|Q\overline{Q}[^1S_0^{(8)}]g\rangle + \mathcal{O}(v^2)|Q\overline{Q}[^3D_J^{(1,8)}]gg\rangle + \cdots$$

$$|\chi_{cJ}\rangle = \mathcal{O}(1)|Q\overline{Q}[^3P_J^{(1)}]\rangle + \mathcal{O}(v)|Q\overline{Q}[^3S_1^{(8)}]g\rangle$$

Factorization between short distance, perturbative, contribution and non-perturbative hadronization, described by non-perturbative matrix elements in limit of large heavy quark mass

NRQCD includes color singlet and color octet matrix elements

- **Two different color singlet matrix elements in NRQCD, one for production and one for decay – can be different even though $\langle\mathcal{O}^3S_1[^3S_1^{(1)}]\rangle \propto |\Psi(0)|^2$ up to order v^4**
- **Perturbative octet amplitudes for $^1S_0^{(8)}$ and $^3P_0^{(8)}$ have the same p_T dependence so they can't be separated, thus a linear combination $\langle\mathcal{O}[^1S_0^{(8)}]\rangle + k\langle\mathcal{O}[^3P_0^{(8)}]\rangle/m_Q^2$ where k is the ratio of the two amplitudes, typically different for high p_T and fixed-target energies**

Combined Color Singlet/Color Octet Global Fit

Global analysis of Butenschon and Kniehl attempts to make global fit to inclusive J/ψ data from RHIC, Tevatron, LHC (all hadroproduction), and HERA (electroproduction)

Fit LO and NLO color singlet (CS) and NRQCD (CS + CO) calculations to data

Instead of fitting octet matrix elements to individual data sets, they attempt to obtain universal matrix elements

- Assume a given value of charm quark mass and scales for calculation
- Fit matrix elements with those parameters
- Determine uncertainties on fit results by keeping matrix elements and quark mass fixed, varying scale parameters by a factor of two around central value

Some caveats:

- Analysis limited to high p_T prompt J/ψ only
- Feed down either neglected or subtracted, assumes that the shape of the χ_c and ψ' distributions same as J/ψ
- No comparison to fixed-target total cross sections
- No attempt to determine how matrix elements depend on quark mass or scale

Global Analysis: PHENIX at RHIC and CDF at the Tevatron

Only NLO CS+CO contributions realize agreement with data

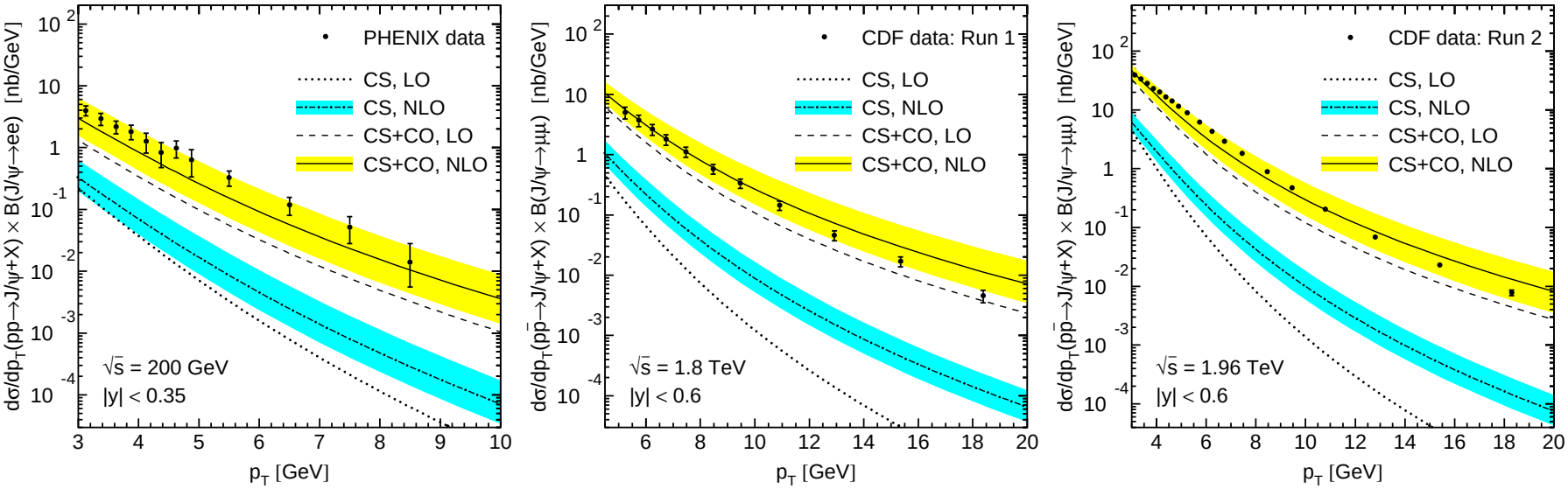

Figure 13: NLO NRQCD fit compared to the PHENIX (RHIC, $\sqrt{s} = 200$ GeV) and CDF (Tevatron, $\sqrt{s} = 1.96$ TeV) data. [Butenschon and Kniehl PRD **84** (2011) 051501]

LO CS+CO Analysis by Sharma and Vitev

Midrapidity LO NRQCD analysis of RHIC, CDF and LHC data

Find similar matrix elements as Butenschon and Kniehl despite being a LO calculation (Butenschon and Kniehl consider lower p_T)

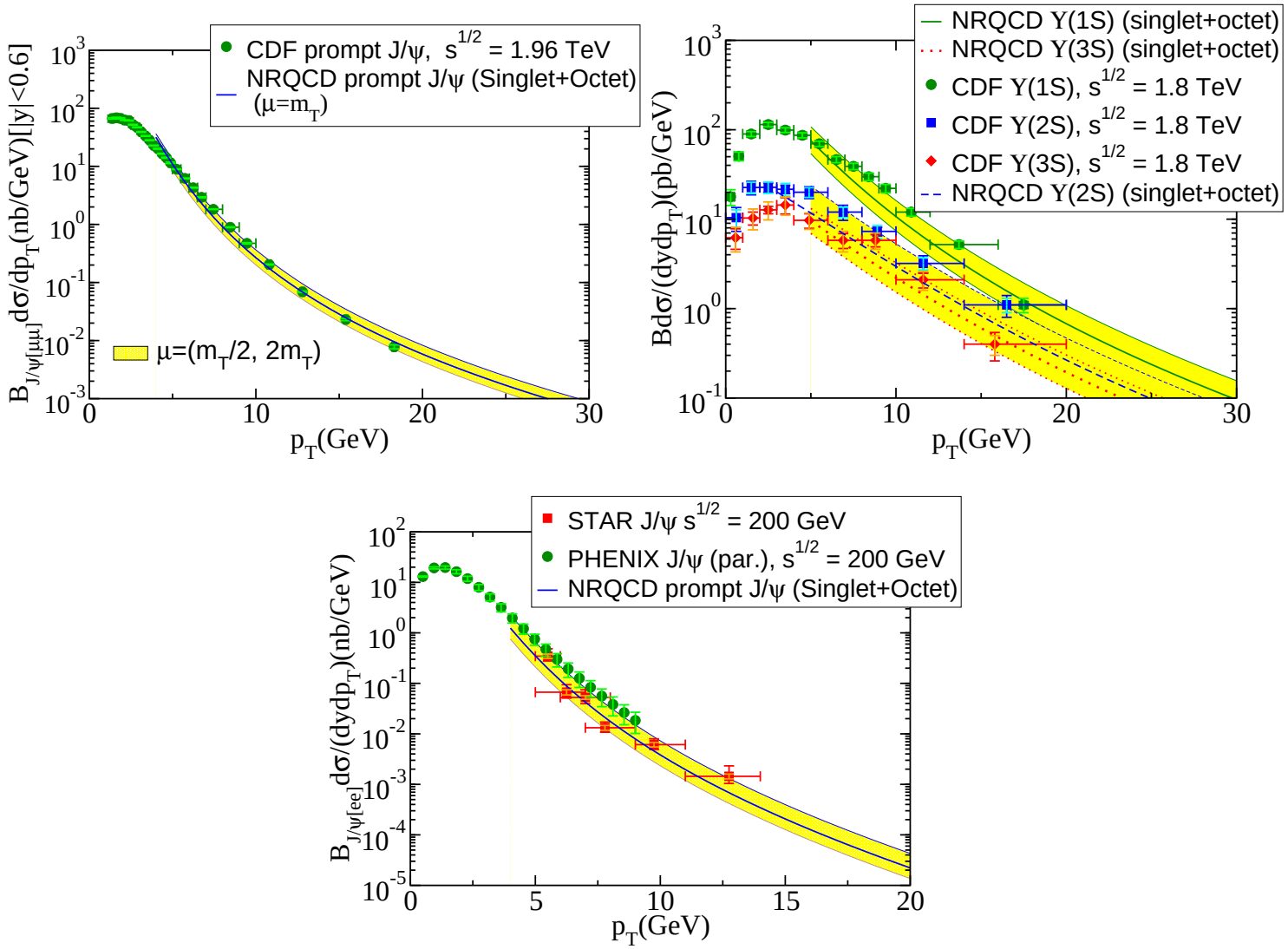

Figure 14: Leading order NRQCD analysis of J/ψ and Υ production at CDF (top) and RHIC (bottom). [Sharma and Vitev, PRC **87** (2013) 044905.]

Polarization Crucial Test of Production Models

At large p_T, the dominant mechanism of quarkonium production is gluon fragmentation into a color octet $Q\overline{Q}$ ($c\overline{c}[^3S_1^{(8)}]$)

Fragmenting gluon is nearly on mass shell and thus transversely polarized, polarization should be retained during hadronization

Polarized cross section, $W \approx 1 + \lambda_\theta \cos^2\theta$ with $\lambda_\theta = 1$, transverse polarization; 0, no polarization; -1, longitudinal polarization

Results shown in helicity frame, LO CSM and NRQCD calculations give transverse polarization, NLO CSM gives longitudinal polarization

Neither gives good description of Tevatron and ALICE data so far

CMS Υ analysis (PRL 110 (2013) 081802) shows no significant polarization, see also work by Faccioli, Lourenco, Seixas, Wohri

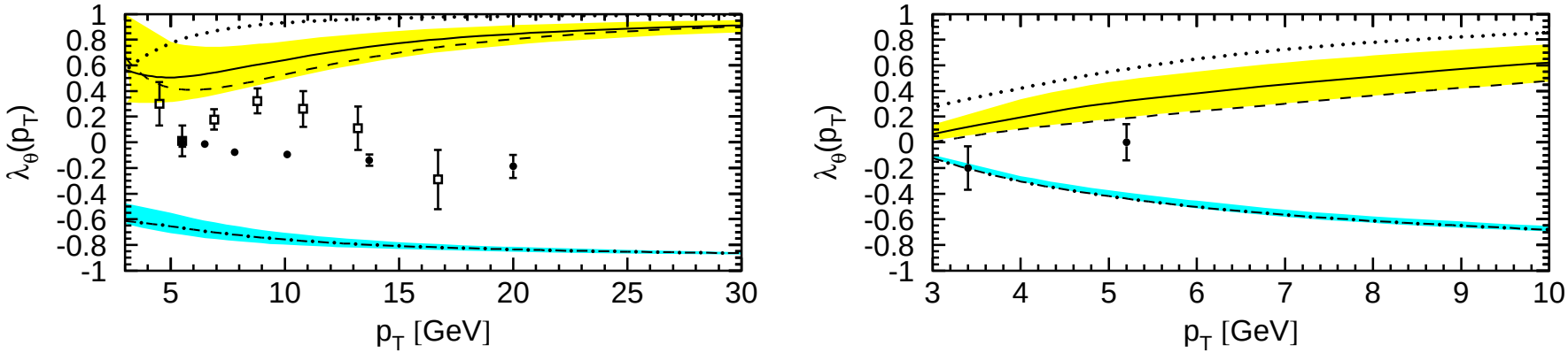

Figure 15: The J/ψ polarization at the Tevatron (left) and at ALICE (right) compared to LO CSM (dotted); NLO CSM (cyan dot-dashed), LO NRQCD (dashed), NLO NRQCD (yellow solid). [Butenschon and Kniehl, PRL **108** (2012) 172002]

Summary of pp

- Multiple ways of calculating higher order open heavy flavor production give similar results
- Collinear factorization seems to work well
- k_T-factorization approach does not necessarily lead to improved agreement with data (similar to saturation model applications to heavy flavor production – the scale is too large to be effective)
- New quarkonium calculations show improved comparison to data but all models have some drawbacks
- Polarization appears to be major stumbling block for all production models

pA and dA: Cold Matter Effects

- **Nuclear Absorption**
- **Shadowing**
- **Energy Loss**

A Dependence of Open Charm and Quarkonium

Open charm production appears independent of A ($N_{\rm bin}$) at midrapidity

Definite A dependence for quarkonium (N.B. E772 data showed little difference between *e.g.* J/ψ and ψ' while later experiments did)

Drell-Yan is effectively independent of A

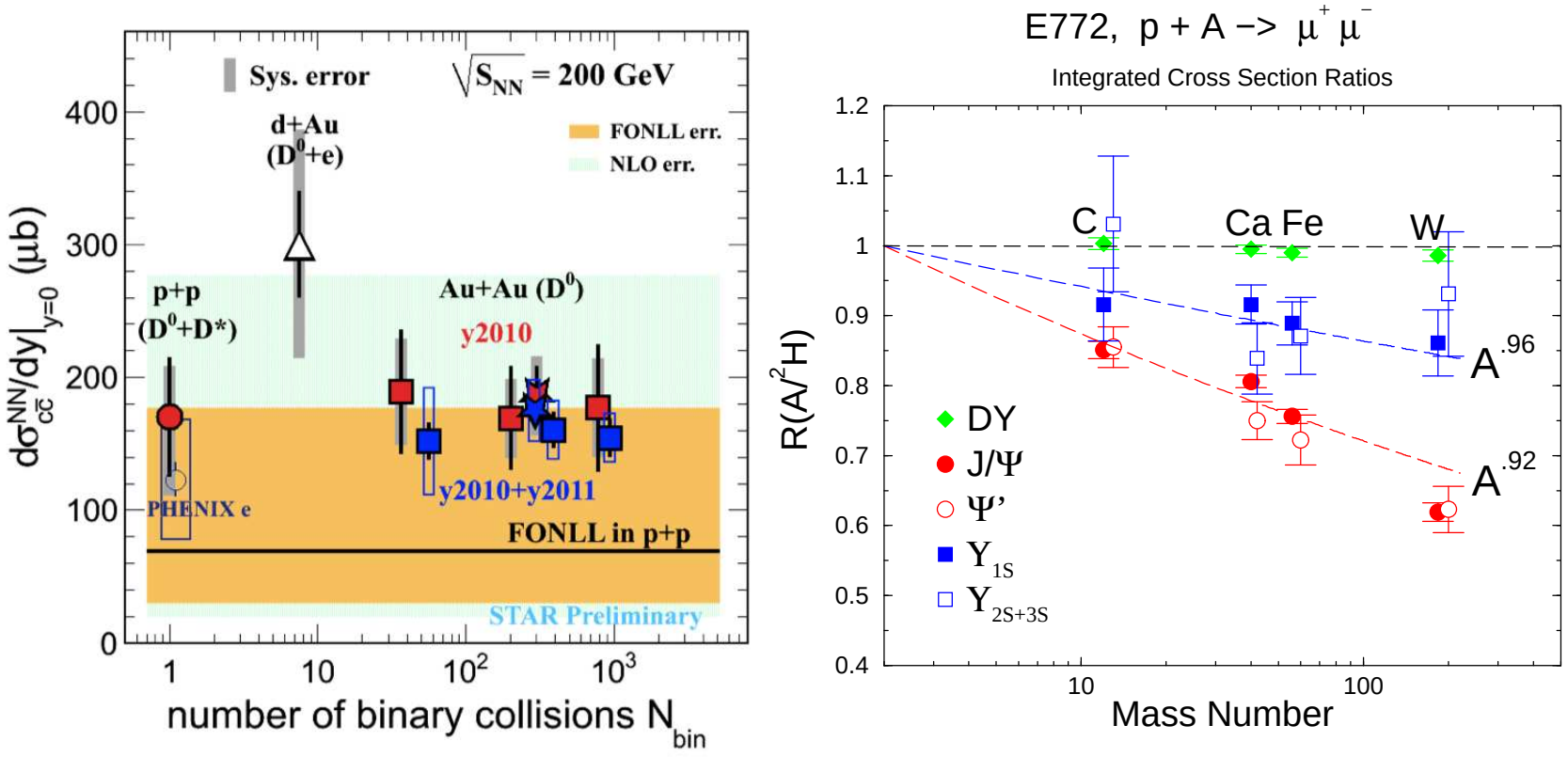

Figure 16: **(Left) The dependence of the open charm cross section on the number of binary collisions measured by the STAR Collaboration at central rapidity. (Right) The A dependence of quarkonium and Drell-Yan production measured by E772.**

E866 Measured Open Charm and J/ψ vs $y_{\rm cm}$

E866 also measured open charm pA dependence using single muons with $p_T^\mu > 1$ GeV/c (unpublished): similar to J/ψ for $y_{\rm cm} > 0.7$

This is one of few data sets for open charm and J/ψ from same experiment – not much available precision data on cold matter effects on open charm production relative to J/ψ

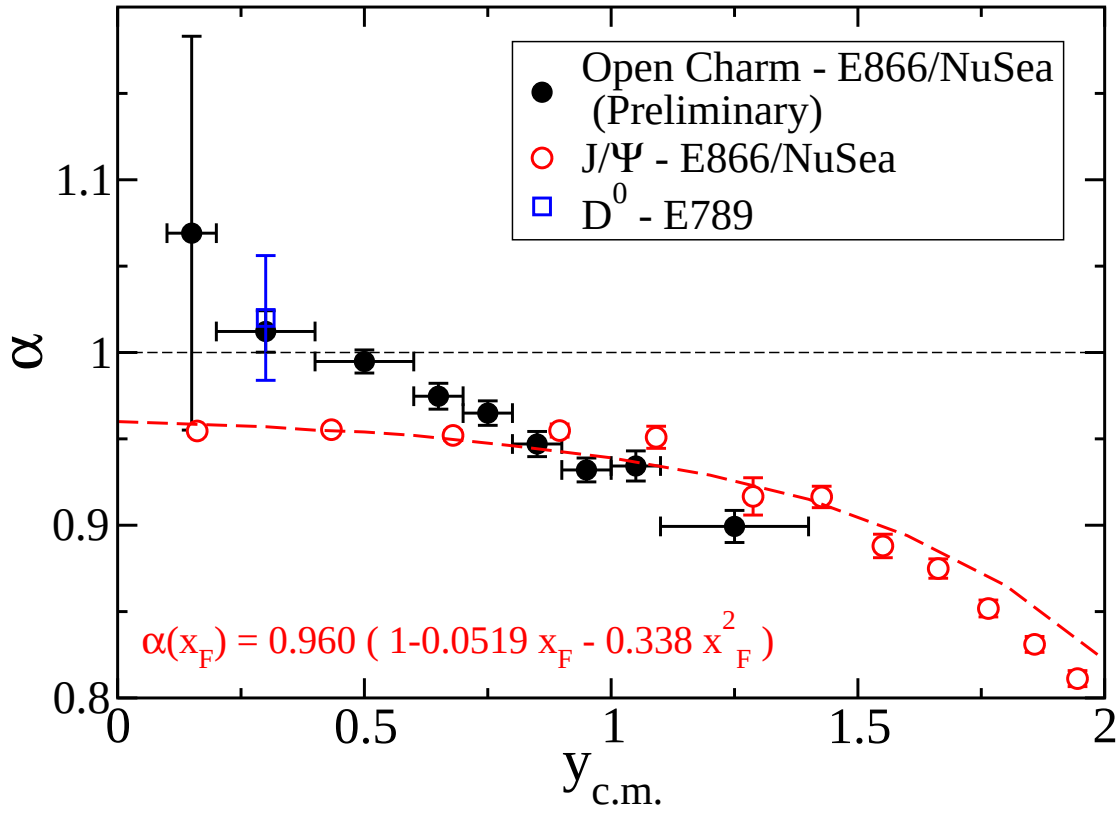

Figure 17: The J/ψ and open charm A dependence as a function of x_F (Mike Leitch).

Cold Nuclear Matter Effects

Important cold nuclear matter effects include:

- **Final-state absorption on nucleons — after $c\bar{c}$ that forms the J/ψ has been produced, pair breaks up in matter due to interactions with nucleons**
- **Initial-state nuclear effects on the parton densities (shadowing) — affects total rate, important as a function of y/x_F**
- **Energy loss — *either* initial-state effect, elastic scatterings of projectile parton before hard scattering creating quarkonium state, need to study Drell-Yan production to get a handle on the strength when shadowing is included — *or* final-state effect, scattering of the $c\bar{c}$ or J/ψ after production — can be related to p_T broadening**
- **Intrinsic heavy flavors**

Shadowing and absorption most important at midrapidity, initial-state energy loss and intrinsic heavy flavor more important at forward rapidity

Production mechanism affects both intimately:

- **Shadowing depends on momentum fraction x of the target (and projectile in AA) which is influenced by how the state was produced: $2 \to 1$ or $2 \to 2$ process**
- **Production affects absorption because singlet and octet states can be absorbed differently**

Cold Matter Effects on Heavy Flavor Production

Production cross section in a pA collision

$$\sigma_{pA}(S,m^2) = \sum_{i,j=q,\overline{q},g} \int_{4m_Q^2/S}^1 \frac{d\tau}{\tau} \int d^2b dz d\epsilon\, dx_1\, dx_2\, \delta(x_1x_2-\tau)\delta(x'_F - x_F - \delta x_F(\epsilon))\delta(x'_F - x_1 + x_2)$$
$$\times P(\epsilon)\, S_A^{\rm abs}(\vec{r},z)\, f_i^p(x_1,\mu_F^2) F_i^A(x'_1,\mu_F^2,\vec{b},z)\, \widehat{\sigma}_{ij}(s,m^2,\mu_F^2,\mu_R^2)$$

Survival probability for absorption of a (proto)charmonium state in nuclear matter

$S_A^{\rm abs}(b,z) = \exp\{-\int_z^\infty dz' \rho_A(b,z')\sigma_{\rm abs}(z-z')\}$

$P(\epsilon)$ is energy loss probability that modifies the x_F of the produced J/ψ state

Nuclear parton densities

$$F_i^A(x,Q^2,\vec{b},z) = \rho_A(s) S^i(A,x,Q^2,\vec{b},z) f_i^p(x,Q^2)\ ;\quad s=\sqrt{b^2+z^2}\ ;\quad \rho_A(s) = \rho_0 \frac{1+\omega(s/R_A)^2}{1+\exp[(s-R_A)/d]}$$

S^i is shadowing parameterization for parton i, *e.g.* EPS09, EKS98, nDSg, DSSZ

With no nuclear modifications, $S^i(A,x,Q^2,\vec{r},z) \equiv 1$

Initial assumption that shadowing strength proportional to nuclear thickness raised to a power n, with appropriate normalization factor

EPS09s parameterization keeps powers $n = 1 \cdots 4$ for A-independent coefficients

$$M_{\rm shad} = 1 - (1 - S^g(x,Q^2)\,)\Big(\frac{T_A^n(b)}{a(n)}\Big)$$

If onset of shadowing is like a step function with a radius R and diffuseness d

$$M_{\rm shad} = 1 - \Big(\frac{1-S^g(x,Q^2)}{a(R,d)(1+\exp((b-R)/d))}\Big)$$

J/ψ A Dependence vs. x_2 and $y_{\rm cm}$

Effective α ($\sigma_{pA}/\sigma_{pp} = A^{\alpha}$) dissimilar as a function of x_2, closer to scaling for $y_{\rm cm}$ (x_1) – higher $\sqrt{s}$ stretches x values relative to rapidity ($x_F = (2m_T/\sqrt{s})\sinh y = x_1 - x_2$)

Translating A dependence into effective absorption cross section, $\sigma_{\rm abs}$, including shadowing effects, shows the x_F dependence of remaining cold matter effects

At negative x_F, HERA-B result suggests a negligible effective $\sigma_{\rm abs}$

Argument for more physics at forward x_F than accounted for by nuclear shadowing: energy loss?

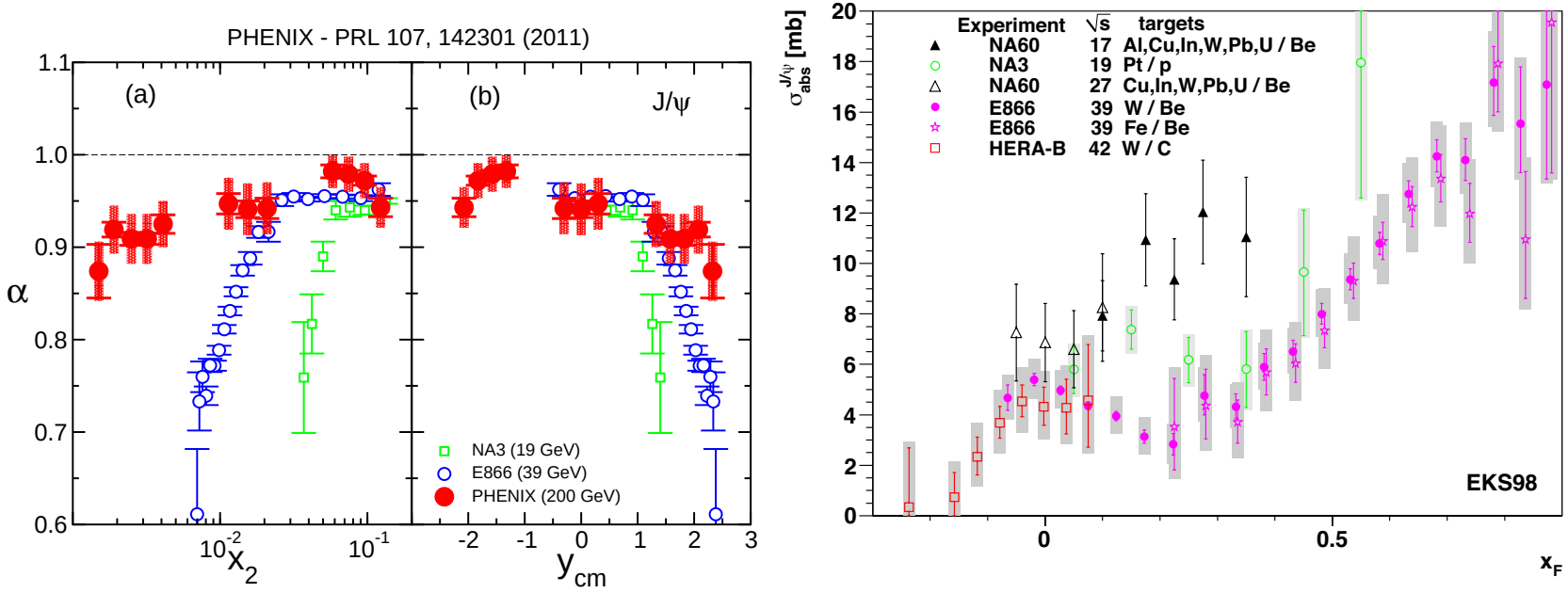

Figure 18: (Left) Comparison of effective α for NA3, E866 and PHENIX. (Mike Leitch) (Right) Comparison of effective $\sigma_{\rm abs}$ for J/ψ (from QWG report, 2010).

Shadowing

Parton Densities Modified in Nuclei

Nuclear deep-inelastic scattering measures quark modifications directly; Drell-Yan and π^0 measurements provide further information

More uncertainty in nuclear gluon distribution, only indirectly constrained by Q^2 evolution, large uncertainties still remain, including LO vs NLO

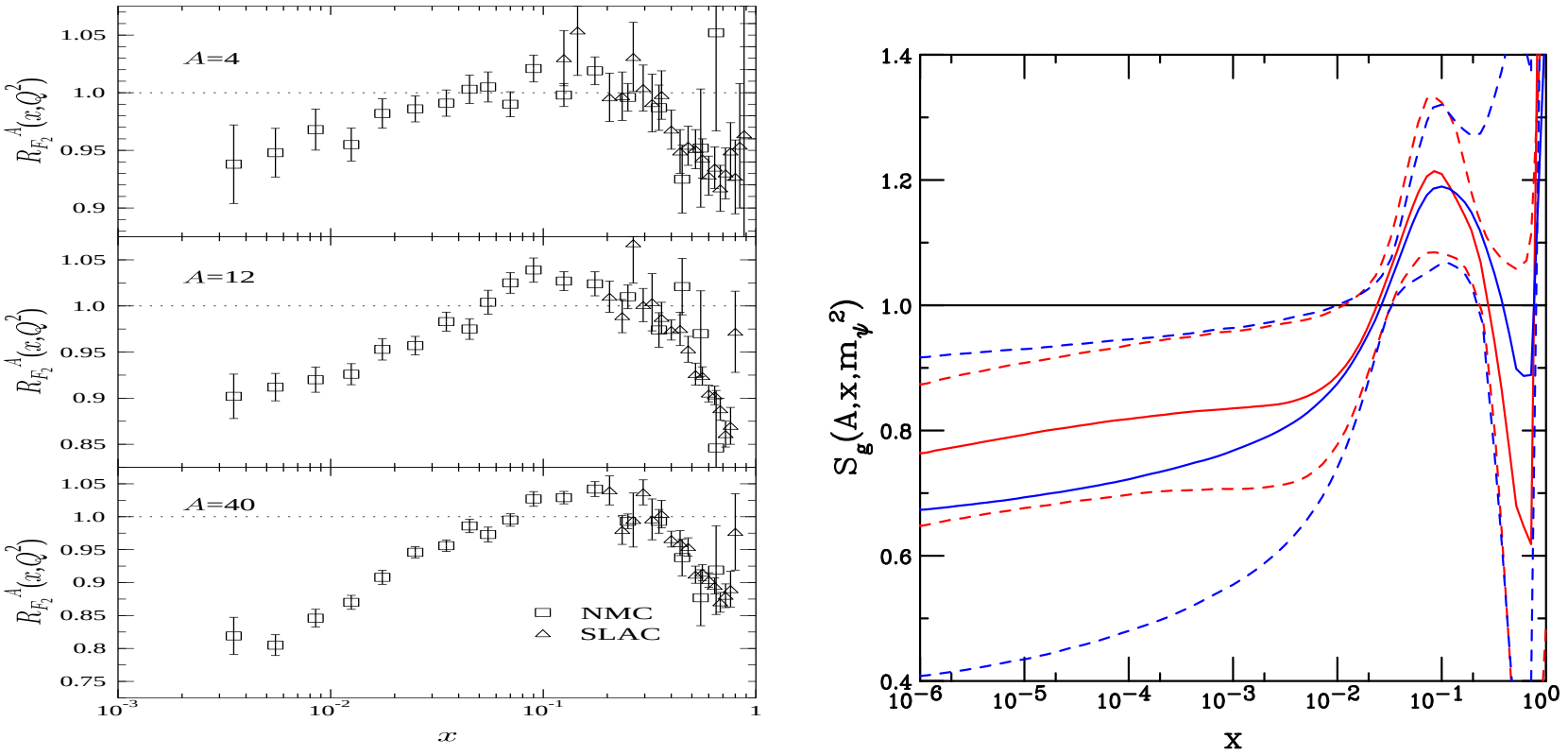

Figure 19: (Left) Ratios of charged parton densities in He, C, and Ca to D as a function of x. [From K.J. Eskola.] (Right) The modification of the gluon densities at LO (blue) and NLO (red) with EPS09, including uncertainties (dashed lines), calculated at m_ψ. (RV)

nPDF Effects on J/ψ in p+Pb at $\sqrt{s_{NN}} = 5$ TeV

EPS09 NLO modifications of J/ψ production, magenta curves show extent of EPS0 uncertainties

Blue curves show the mass and scale uncertainties relative to the central value, smaller than nPDF uncertainty

Rapidity dependence assumes that proton moves to the right
Forward/backward ratio independent of pp normalization

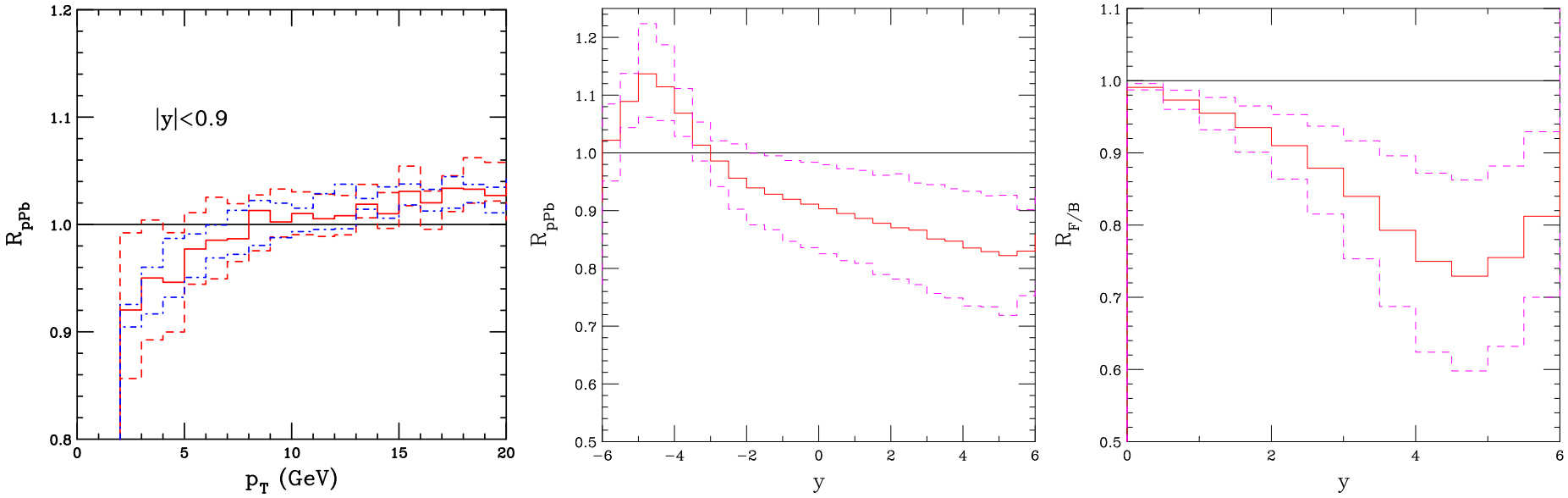

Figure 20: **The $R_{p\mathrm{Pb}}$ ratios for J/ψ as a function of p_T (left) and y (center). The right hand plot shows the forward/backward ratio in minimum bias collisions. The dashed red histogram shows the EPS09 uncertainties while the dot-dashed blue histogram shows the dependence on mass and scale. The pp denominator is also calculated at 5 TeV (which isn't available experimentally) and does not take the rapidity shift in p+Pb into account. RV**

Saturation?

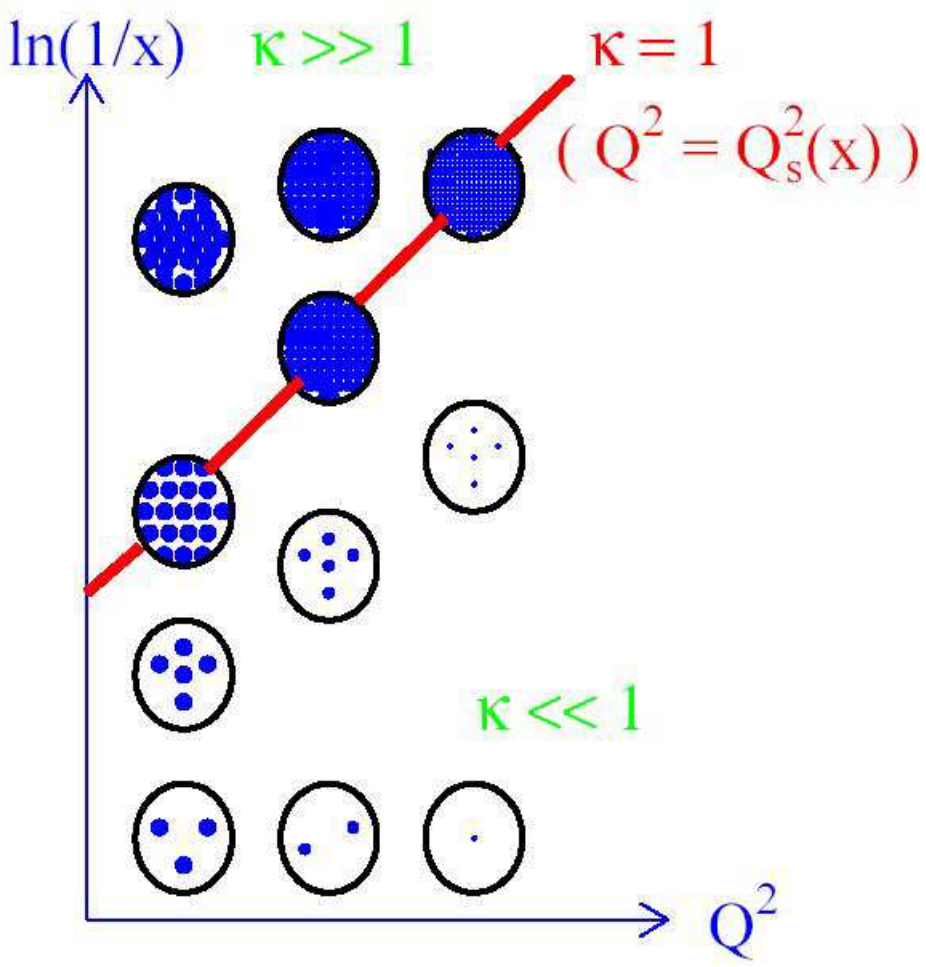

Saturation condition: when the gluon density, ρ_g, is sufficiently high, recombination of gluons $(2 \to 1)$ competes with emission of new partons $(1 \to 2)$ $\rho \sim 1/\alpha_s$

Packing factor: fraction of how much of nucleon/nuclear disk is packed with partons,
$\kappa = \sigma_{\rm dipole}/\pi R^2$, $\sigma_{\rm dipole} \propto F_2(x, Q^2)/Q^2$

$Q_{\rm sat}$ grows with increasing $\sqrt{s}$ and decreasing x

In nuclei $Q_{\rm sat}$ increases by $A^{1/3}$

Scale of J/ψ and open charm likely above $Q_{\rm sat}$

Stronger Than Linear Impact Parameter Dependence?

RHIC minimum bias (impact-parameter integrated shadowing) d+Au data agrees with EPS09 shadowing and 4 mb absorption cross section

The R_{CP} ratio does not agree with the impact-parameter dependent shadowing calculation at forward rapidity because the peripheral result is overestimated

Correlation between uncertainties allows shifts (forward up + backward down)

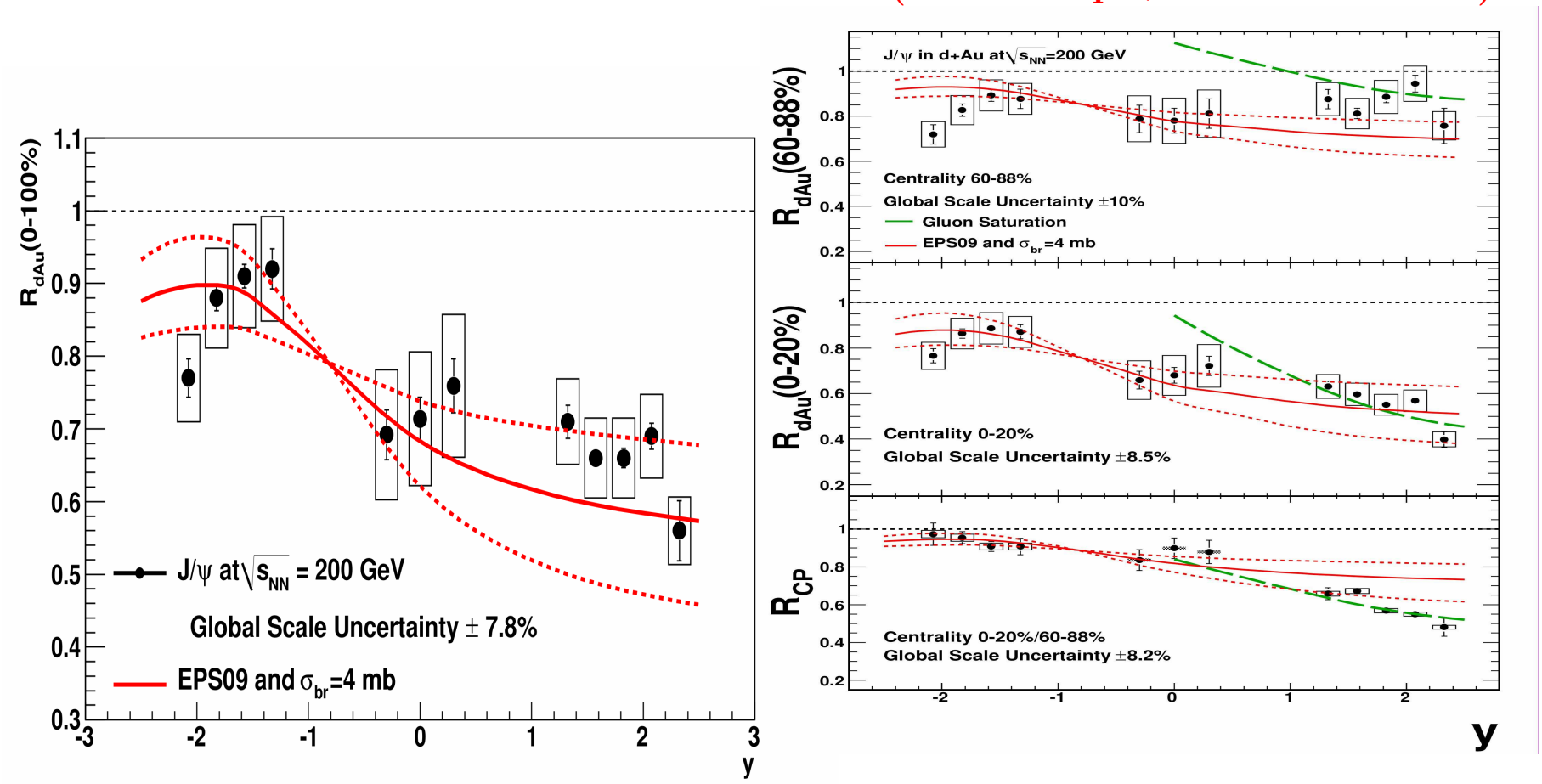

Figure 21: The PHENIX data compared to calculations of EPS09 shadowing including uncertainties and a constant absorption cross section of 4 mb. Left: the minimum bias result. Right: Including impact-parameter dependent shadowing in the $60-88\%$ centrality (top) and $0-20\%$ centrality (middle) bins. The lower panel shows the central-to-peripheral ratio. The dashed curves shows a gluon saturation calculation.

Impact Parameter Dependence of Shadowing on J/ψ?

Onset of shadowing with impact parameter r_T consistent with shadowing effects concentrated in core of nucleus where nucleons are more densely packed

Sharp onset of shadowing gives smaller effective absorption cross sections than linear dependence but does not change overall shape

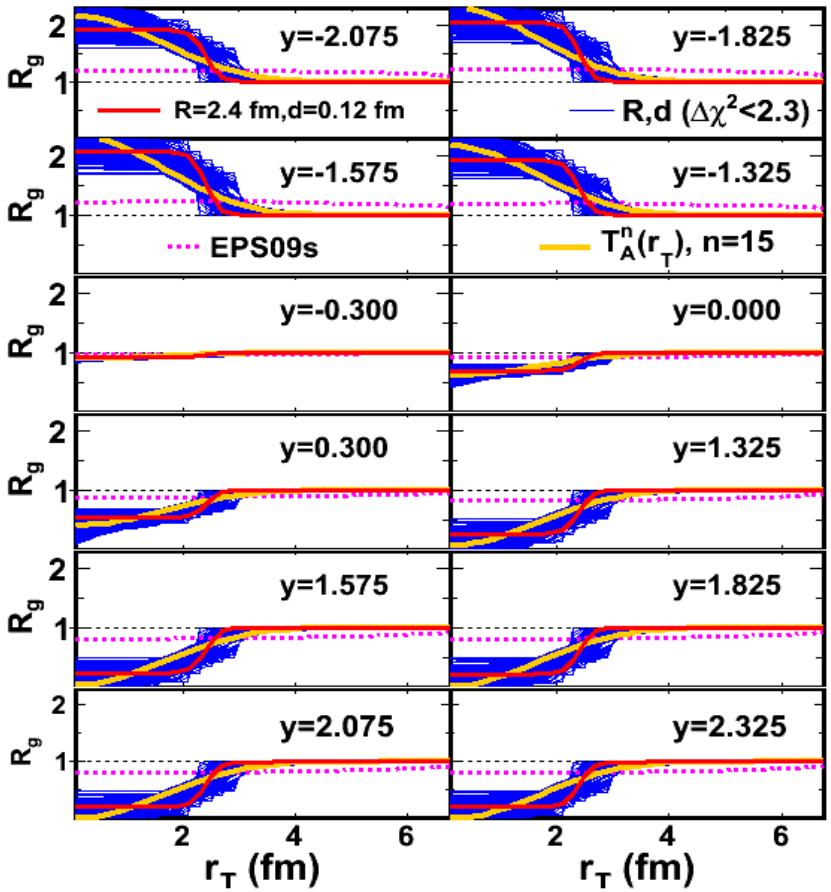

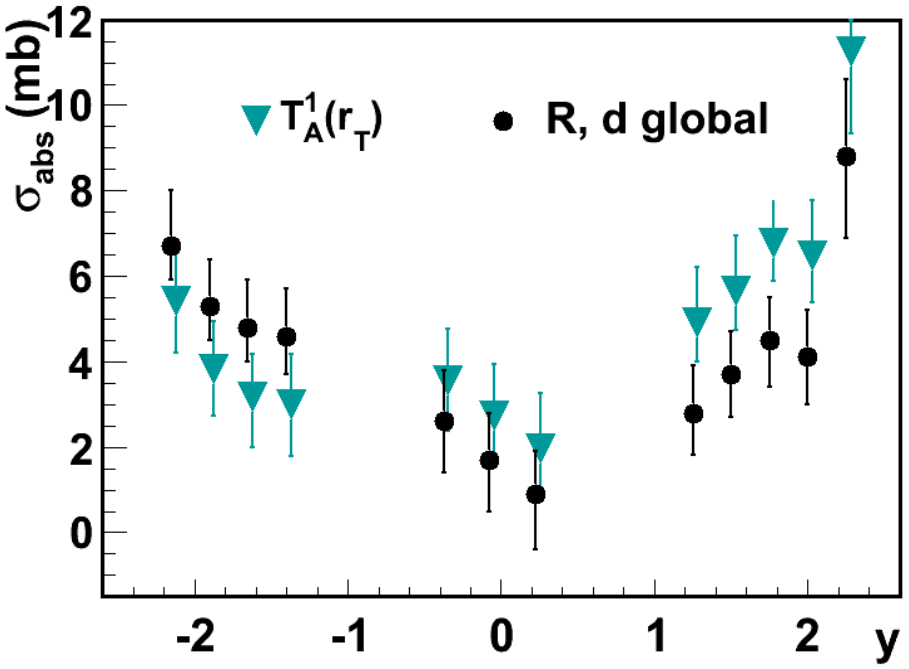

Figure 22: (Left) The gluon modification from the best fit global R and d (solid red line), along with results for all combinations of R and d within the $\Delta\chi^2 = 2.3$ fit contour (thin blue lines). The modification from $T_A^n(r_T)$ ($n = 15$) is shown by the solid orange line. The dashed magenta line is the EPS09s impact parameter dependence. (Right) Comparison of $\sigma_{\rm abs}$ extracted from the PHENIX data assuming a linear dependence on nuclear thickness with those extracted using global values of R and d. [D. McGlinchey, A. D. Frawley and RV, Phys. Rev. C **87** (2013) 054910.]

Nuclear Absorption

Energy Dependence of $\sigma_{\rm abs}^{J/\psi}$

At midrapidity, there seems to be a systematic decrease of the absorption cross section with energy independent of shadowing, trend continues at RHIC

$\sigma_{\rm abs}^{J/\psi}(y_{\rm cms}=0)$ extrapolated to 158 GeV is significantly larger than measured at 450 GeV, underestimating "normal nuclear absorption" in SPS heavy-ion data

Calculations confirmed by NA60 pA measurements at 158 GeV (QM09)

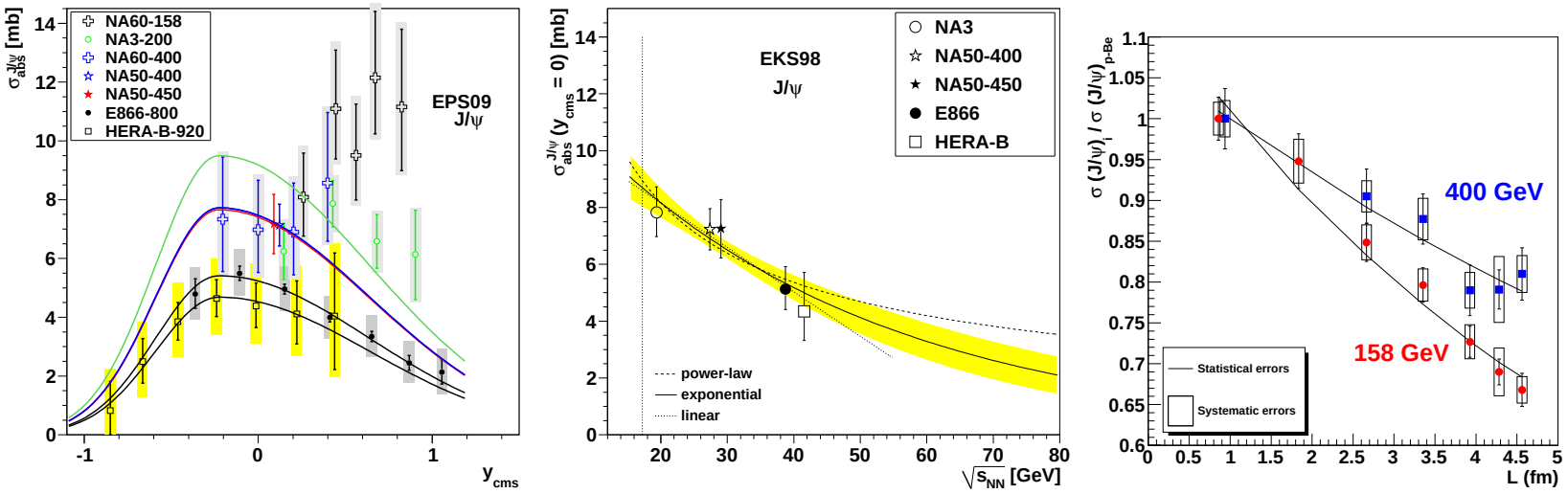

Figure 23: Left: Dependence of $\sigma_{\rm abs}^{J/\psi}$ on $y_{\rm cms}$ for all available data sets including EPS09 shadowing. The shape of the curves is fixed by the E866 and HERA-B data. [Lourenço, RV, Wöhri] Middle: The extracted energy dependence of $\sigma_{\rm abs}^{J/\psi}$ at midrapidity for power law (dashed), exponential (solid) and linear (dotted) approximations to $\sigma_{\rm abs}^{J/\psi}(y=0,\sqrt{s_{NN}})$ using the EKS98 shadowing parameterization with the CTEQ61L parton densities. The band around the exponential curve indicates the uncertainty in the extracted cross sections at $x_F \sim 0$ from NA3, NA50 at 400 and 450 GeV, E866 and HERA-B. The vertical dotted line indicates the energy of the Pb+Pb and In+In collisions at the CERN SPS. [Lourenço, RV, Wöhri] Right: The J/ψ cross section ratios for pA collisions at 158 GeV (circles) and 400 GeV (squares), as a function of L, the mean thickness of nuclear matter traversed by the J/ψ. [Arnaldi, Cortese, Scomparin]

$\sigma_{\rm abs}$ Grows with time $c\bar{c}$ Spends Traversing Nucleus

Mid- and backward rapidity J/ψ at $\sqrt{s_{NN}} = 200$ GeV (longer $\tau = L/\gamma$) dominated by conversion of color octet $c\bar{c}$ pair to color singlet J/ψ by gluon emission

$$\sigma_{\rm abs}(\tau) = \sigma_1 \Big(\frac{\sqrt{s}}{10\ GeV}\Big)^{0.4} \Big(\frac{r_{c\bar{c}}(\tau)}{r_{\rm J/\psi}}\Big)^2 \qquad r_{c\bar{c}}(\tau) = r_0 + v_{c\bar{c}}\tau \text{ for } r_{c\bar{c}}(\tau) < r_\psi$$

Different physics at forward rapidity where conversion takes place outside target

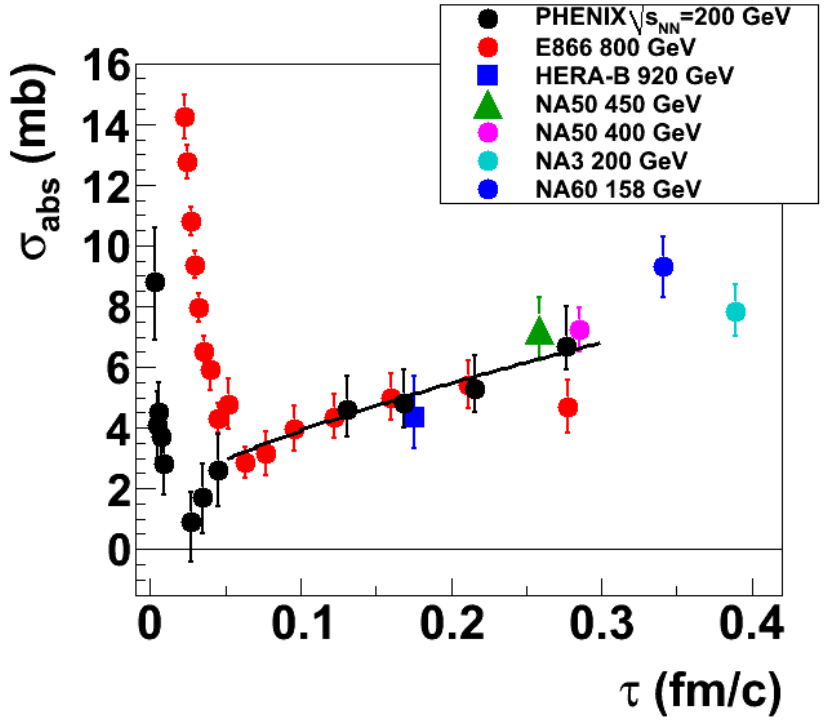

Figure 24: The effective $c\bar{c}$ breakup cross section as a function of the proper time spent in the nucleus, τ. The values were extracted from PHENIX $\sqrt{s_{NN}} = 200$ GeV d+Au data after correction for shadowing using EPS09 and from fixed-target p+A data measured by E866 at 800 GeV, by HERA-B at 920 GeV, by NA50 at 450 GeV and 400 GeV, by NA3 at 200 GeV, and by NA60 at 158 GeV. In all fixed-target cases, the EKS98 parameterization was used. The curve is calculated based on octet-to-singlet conversion inside the nucleus. [D. McGlinchey, A. D. Frawley and RV, Phys. Rev. C **87** (2013) 054910.]

A Dependence of J/ψ and ψ' Not Identical: Size Matters

Color octet mechanism suggested that J/ψ and ψ' A dependence should be identical — Supported by large uncertainties of early data

More extensive data sets (NA50 at SPS, E866 at FNAL) show clear difference at midrapidity [NA50 ρL fit gives $\Delta\sigma = \sigma^{\psi'}_{\rm abs} - \sigma^{J/\psi}_{\rm abs} = 4.2 \pm 1.0$ mb at 400 GeV, 2.8 ± 0.5 mb at 450 GeV for absolute cross sections]

Suggests we need to include formation time effects

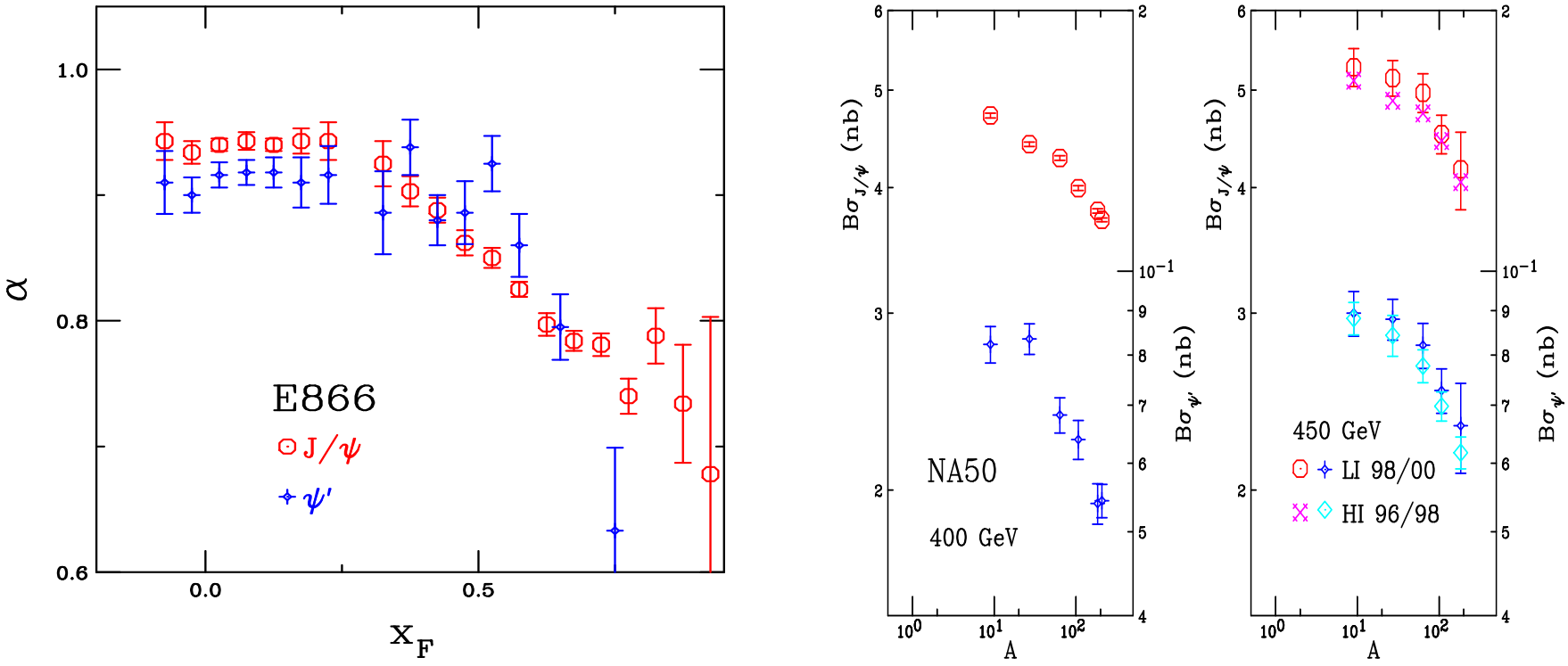

Figure 25: **The J/ψ A dependence (left) as a function of x_F at FNAL ($\sqrt{s_{NN}} = 38.8$ GeV) and (right) and a function of A at the SPS (NA50 at $p_{\rm lab} = 400$ and 450 GeV) for J/ψ and ψ' production.**

PHENIX Has Measured $R_{\rm dAu}$ for ψ' and χc

$R_{\rm dAu} \sim 0.77 \pm 0.02 \pm 0.16$, $(0.81 \pm 0.12 \pm 0.23)$, $0.77 \pm 0.41 \pm 0.18$, $0.54 \pm 0.11^{0.16}_{-0.19}$ for inclusive (direct) J/ψ, χ_c and ψ' respectively

χ_c A dependence never measured in fixed-target experiments, singlet production of χ_c could lead to different absorption pattern

Dramatic difference in $N_{\rm bin}$ dependence of J/ψ and ψ', not seen previously in pA but never measured vs. centrality before

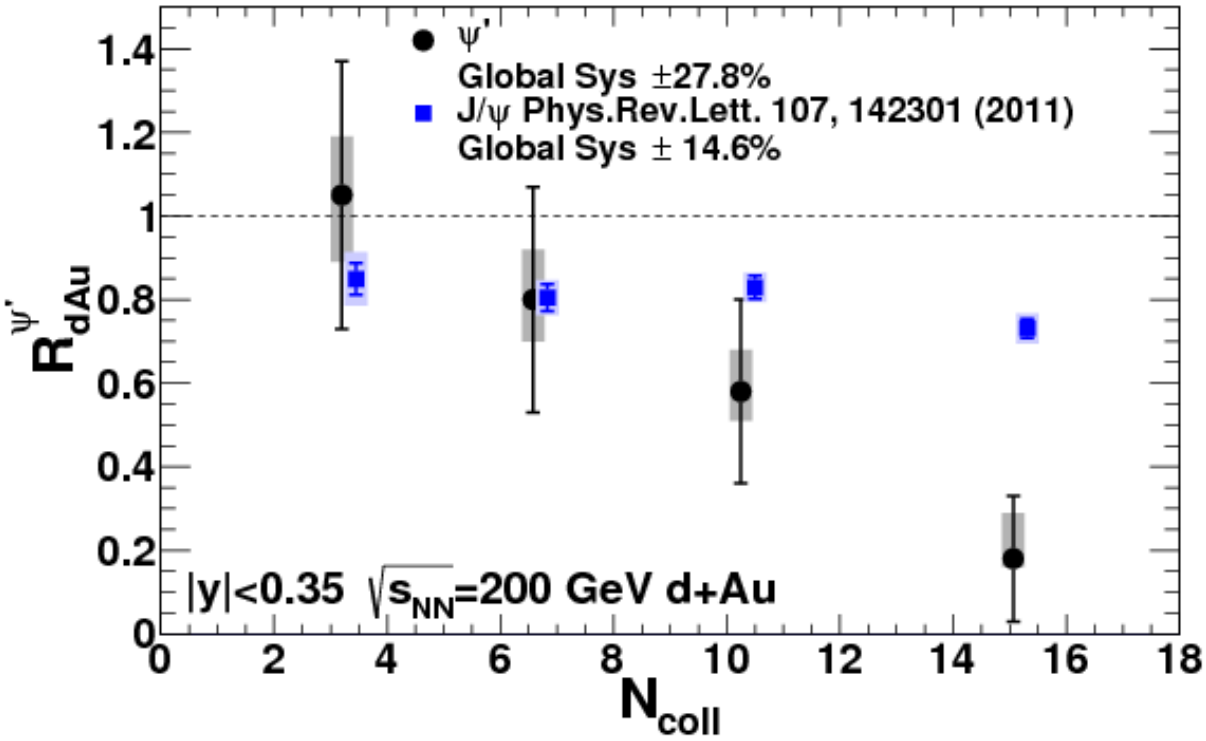

Figure 26: The J/ψ and ψ' $N_{\rm coll}$ dependence as reported by PHENIX. [arXiv:1305.5516]

Energy Loss

Final-State Energy Loss (Arleo and Peigne)

Arleo and Peigne (arXiv:1212.0434) fit path-length dependent energy loss parameter to E866 data and uses the same parameter for other energies

$$\frac{1}{A}\frac{d\sigma_{pA}(x_F)}{dx_F} = \int_0^{E_p-E} d\epsilon P(\epsilon)\frac{d\sigma_{pp}(x_F+\delta x_F(\epsilon))}{dx_F}$$

The pp result is calculated without any production model, $d\sigma_{pp}/dx = (1-x)^n/x$ where n is fit to data, $n \sim 34$ at 5 TeV, large backward effect caused by shift of x_F distribution in pA

Does not violate bounds on energy loss because it is final-state effect

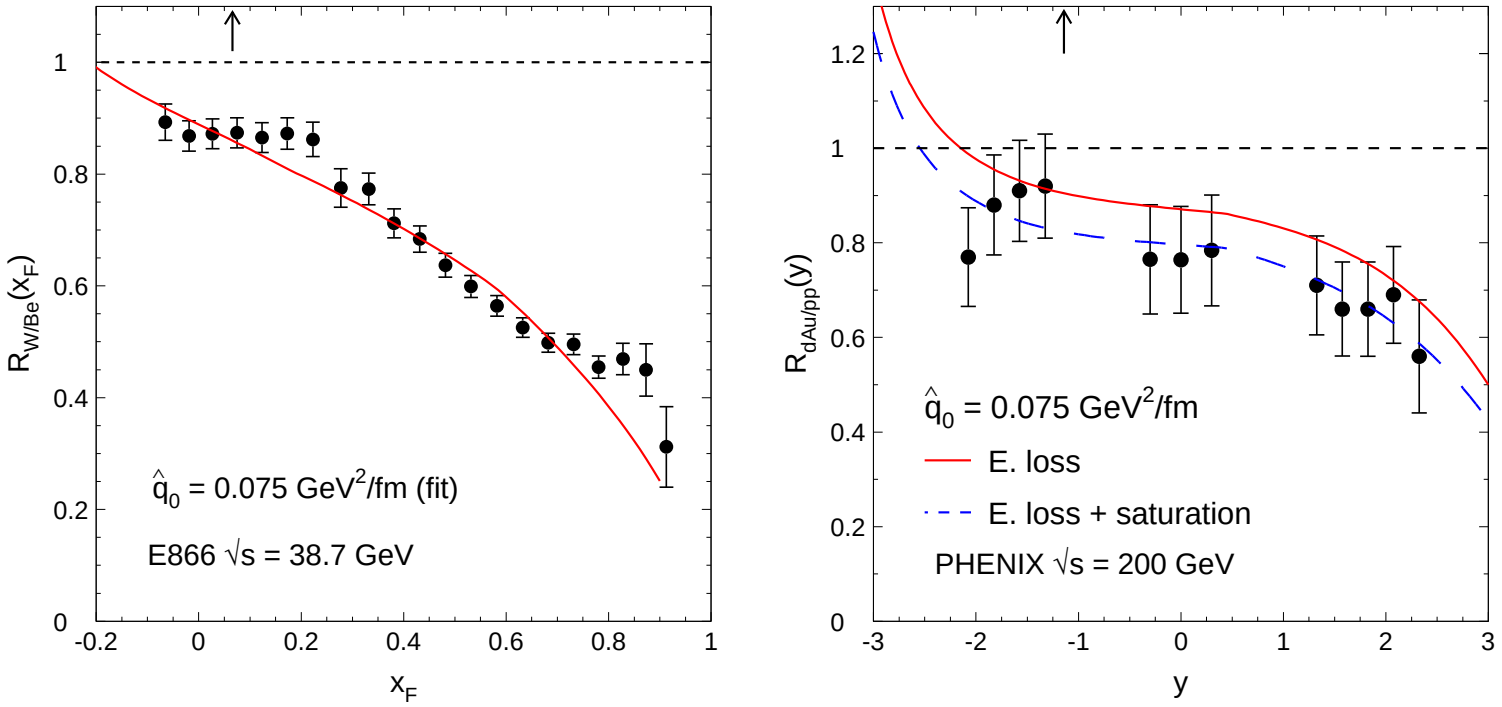

Figure 27: E866 J/ψ suppression in pW/pBe collisions at $\sqrt{s} = 38.8$ GeV (left) and the PHENIX $R_{\rm dAu}$ at $\sqrt{s} = 200$ GeV collisions (right) [Arleo and Peigne].

Summary of pA/dA

- **Little known about open heavy flavor CNM effects; open charm could be similar to J/ψ away from midrapidity a la unpublished E866 data**
- **J/ψ CNM effects studied for long time but still no coherent picture**
- **χ_c A dependence should be part of complete study but still virtually unknown**
- **Υ CNM effects expected to be weaker but still significant**

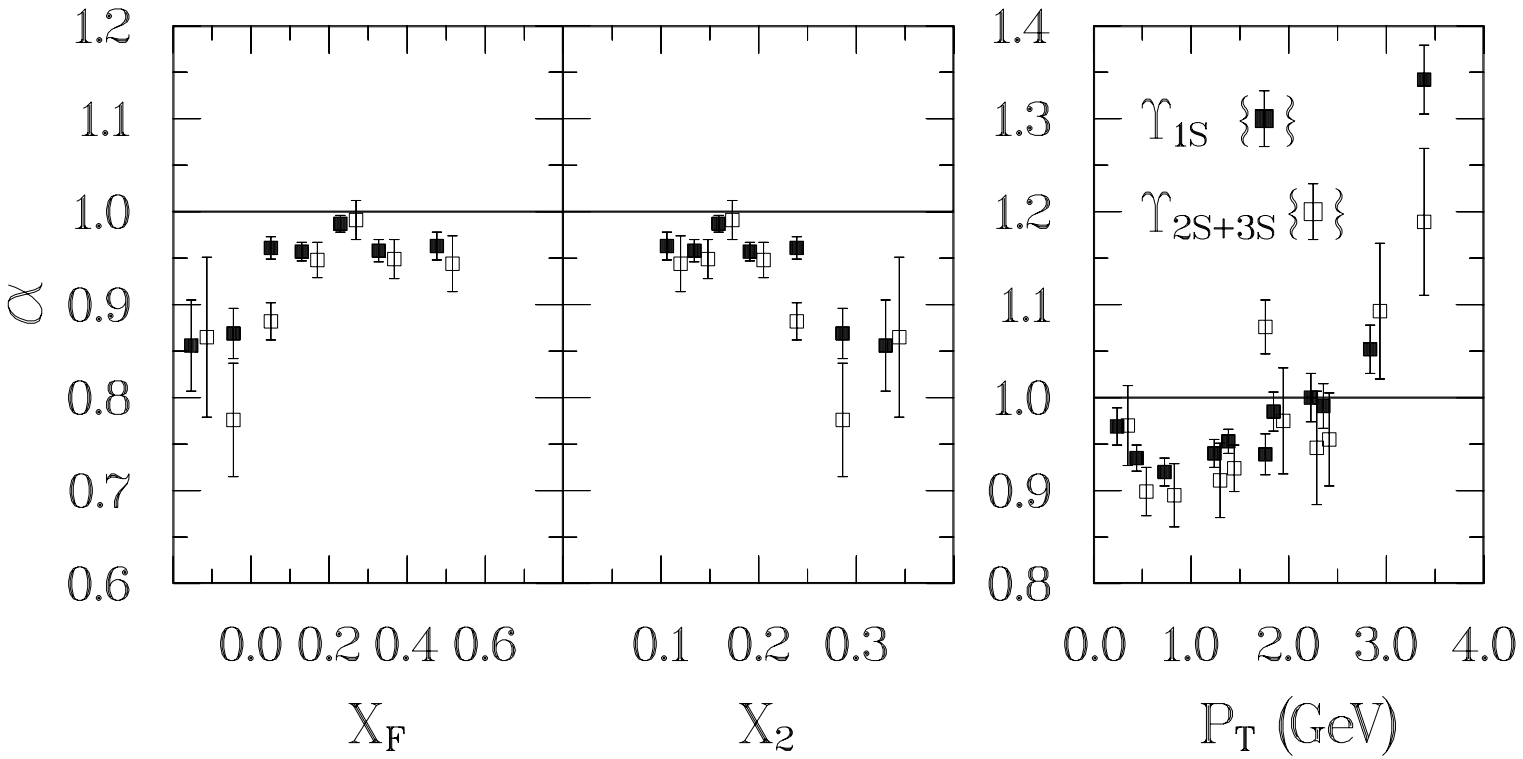

AA Collisions: Hot Matter

- **Quarkonium**
  - **Cold Matter in AA**
  - **Energy Loss**
  - **Lattice-Based Results and Potential Models (arXiv:1302.2180)**
- **Open Heavy Flavor**
  - **Langevin Approaches (with Recombination)**
- **Setting Proper Normalization for Quarkonium Suppression**

Cold Matter Effects on Quarkonium

Shadowing in AA Convolution of pA and Ap

NLO gluon parameterization gives narrower uncertainty on shadowing

Au+Au result at RHIC is convolution of $R_{\mathrm{d+Au}}$ and $R_{\mathrm{Au+d}}$ assuming collinear factorization and no additional effects

NLO convolution gives stronger effect at forward rapidity than at midrapidity, similar to PHENIX data

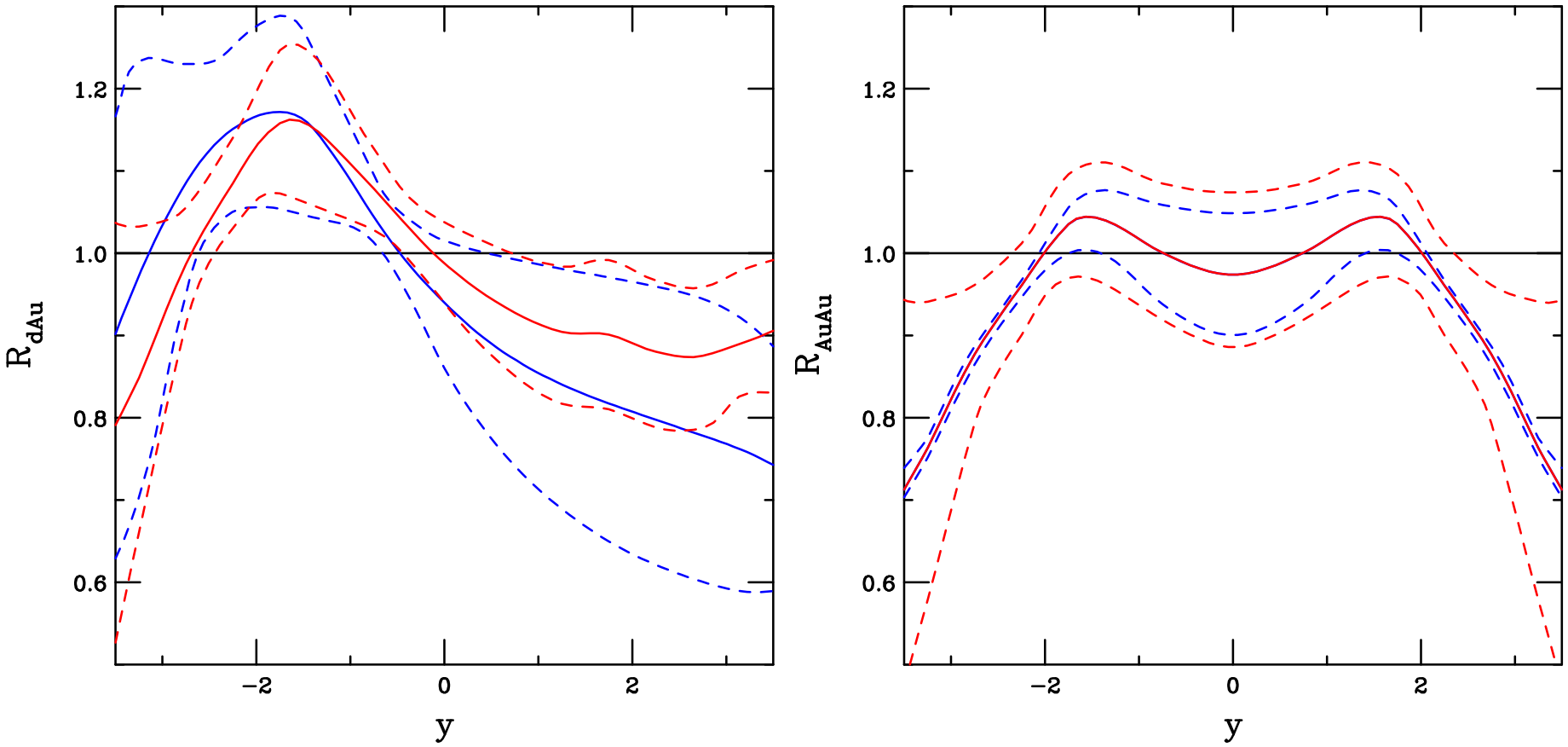

Figure 28: (Left) Comparison of LO (blue) and NLO (red) shadowing results for R_{dAu}. (Right) Comparison of uncertainties due to shadowing (red) and mass/scale values (blue) for R_{AuAu}. Both results are calculated at at $\sqrt{s_{NN}} = 200$ GeV with the EPS09 parameterizations.

Ultraperipheral Collisions Cleaner Shadowing Measure

Ultraperipheral collisions free of final-state effects as well as absorption because nuclei do not touch
EPS09 gives rather good agreement with ALICE midrapidity data

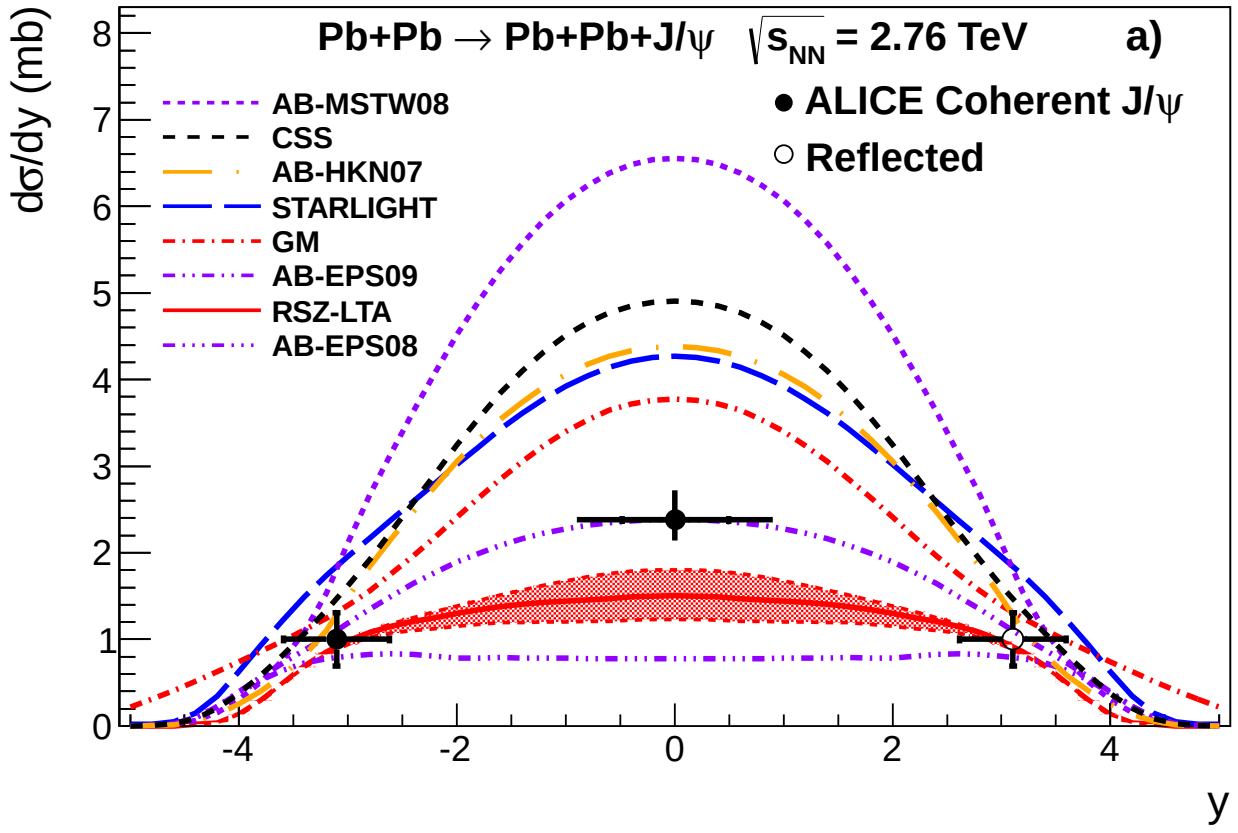

Figure 29: Coherent photoproduction of J/ψ in ultraperipheral Pb+Pb collisions at $\sqrt{s_{NN}} = 2.76$ TeV measured by ALICE in central and forward rapidities compared to various shadowing parameterizations. [From arXiv:1305.1467.]

p_T Dependence Accessible in AA at NLO

Small enhancement at large p_T at RHIC energy due to shadowing, larger enhancement in Au+Au over d+Au

Assuming Cronin enhancement in pA and AA would increase effect
Shadowing alone does not describe data, other hot matter effects required

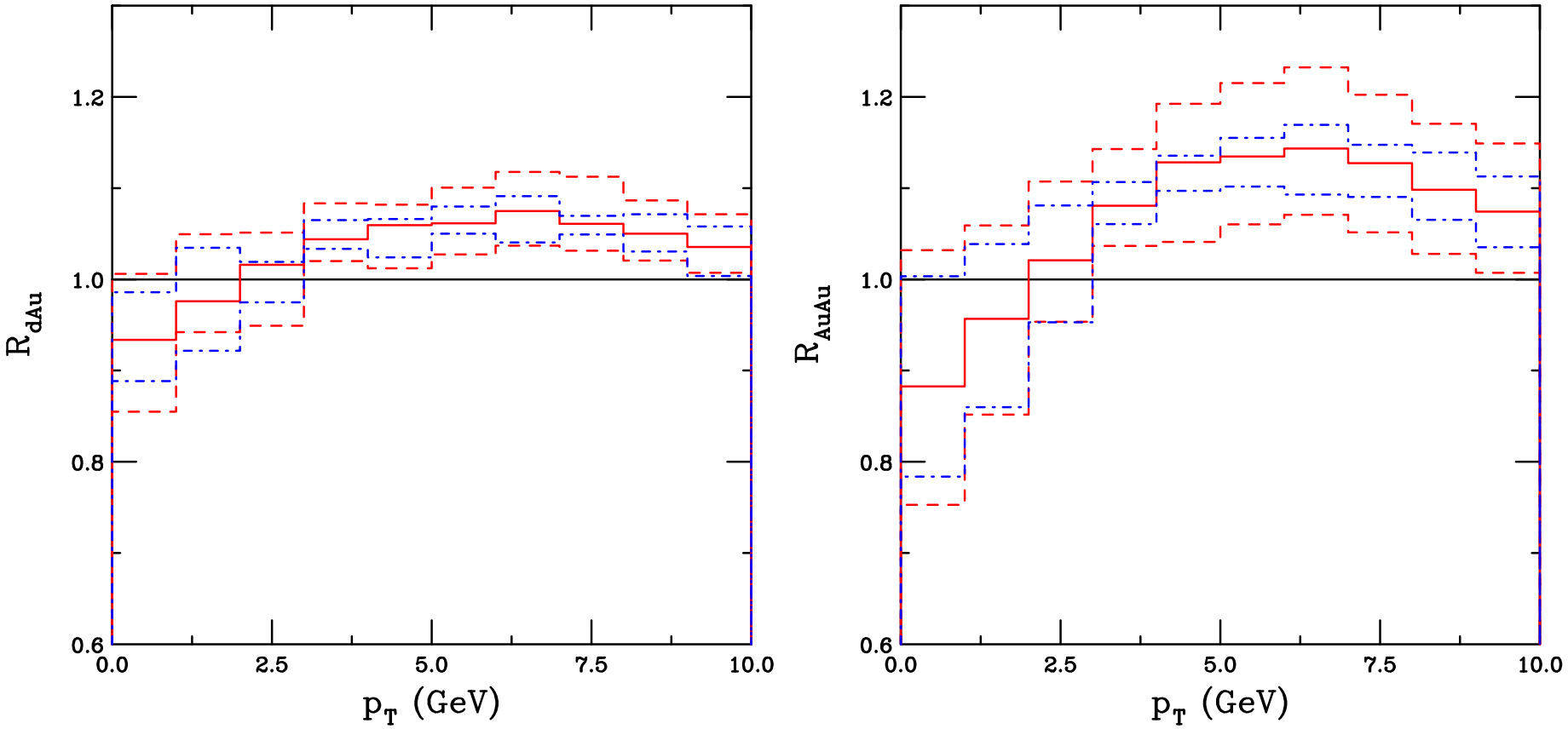

Figure 30: The p_T dependence of the nuclear modification factor is shown for d+Au (left) and Au+Au (right) collisions. Only shadowing effects are included. Both results are calculated at at $\sqrt{s_{NN}} = 200$ GeV with the EPS09 parameterizations.

Sharma and Vitev Energy Loss w & w/out Cronin

CNM effects include dynamical shadowing (power suppressed resummation shifts x values in PDFs) and initial state energy loss, $\epsilon = \Delta E/E$, PDFs evaluated at $x/(1-\epsilon)$ instead of x

Collisional dissociation calculated with $T = 0$ wavefunctions, no thermalization

Suppression rate based on competition between formation and dissociation times of color singlets, GLV quenching used for color octets

Cronin effect, $\langle k_T^2 \rangle_{AB} = \langle k_T^2 \rangle_{pp} + \langle k_T^2 \rangle_{\rm IS}$ overestimates R_{AA}

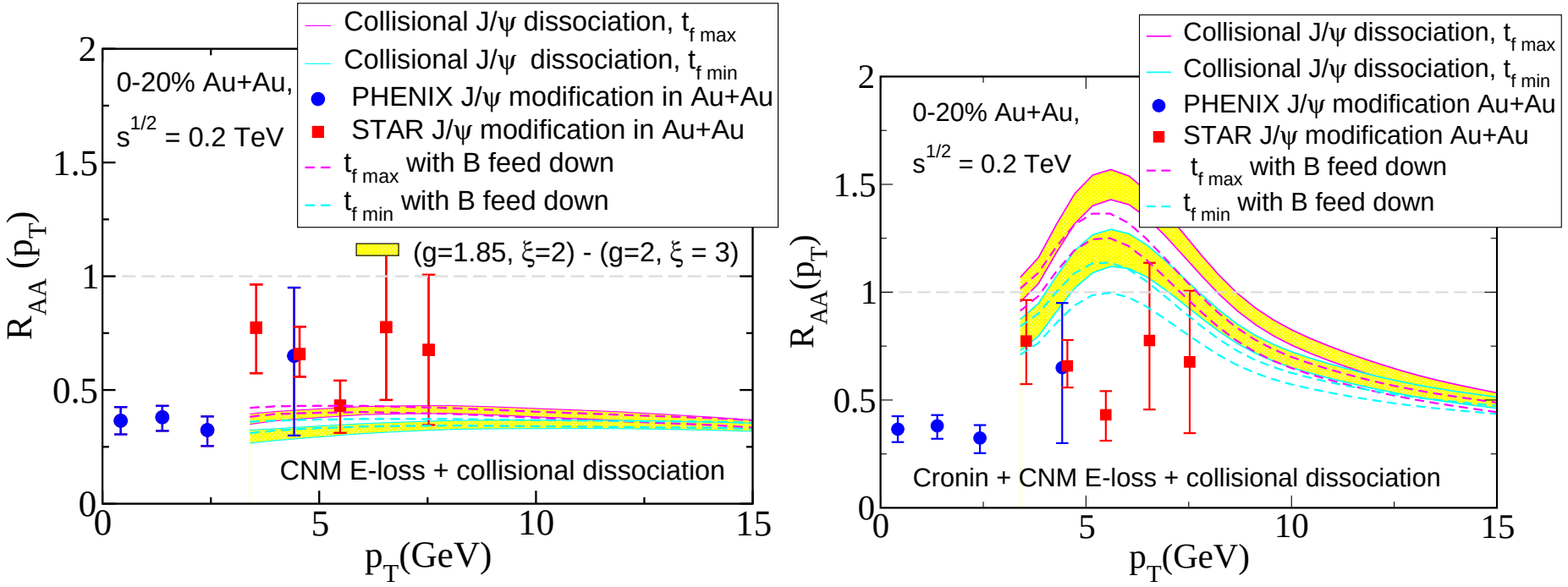

Figure 31: The p_T dependence of the nuclear modification factor is shown for d+Au (left) and Au+Au (right) collisions. Only shadowing effects are included. Both results are calculated at at $\sqrt{s_{NN}} = 200$ GeV with the EPS09 parameterizations.

Lattice-Related Results

- **Finite temperature quarkonium results all based on lattice calculations**
- **SU(N) pure glue has a broken center symmetry associated with deconfinement so SU(N) has a true phase transition**
- **Dynamical quarks break this symmetry so a true deconfinement transition temperature cannot be defined in real QCD**

Color Screening in SU(N)

Pure glue order parameters of phase transition are expectation values of Polyakov loop and the loop correlator

$$L(T) = \langle \frac{1}{N} \mathrm{Tr} W(\vec{x}) \rangle, \; W(\vec{x}) = \prod_{\tau=0}^{N_\tau - 1} U_0(\tau, \vec{x})$$

$$C_{PL}(r,T) = \frac{1}{N^2} \langle \mathrm{Tr} W(r) \mathrm{Tr} W(0) \rangle$$

$L(T) = 0$ in confined phase, $\neq 0$ (finite) in deconfined phase

Correlator C related to free energy of static $Q\overline{Q}$ pair

As $T \to 0$, free energy is equivalent to static potential

In real QCD the static $Q\overline{Q}$ can already be screened in vacuum by light dynamical quarks: pure glue has higher T than with quarks

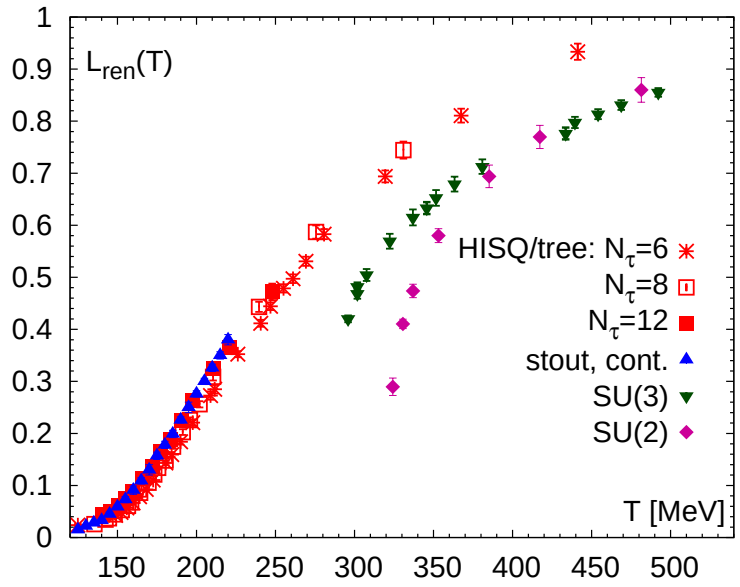

Figure 32: The Polyakov loop as a function of temperature in 2+1flavor QCD and in pure gauge theory. [arXiv:1302.2180]

Free Energy of $Q\overline{Q}$ Pair

At leading order, the free energy of a static $Q\overline{Q}$ pair is

$$F(r,T) = -\frac{1}{N^2}\frac{\alpha_s^2}{r^2}\exp(-2m_D r) - \frac{N^2-1}{2N}\alpha_s m_D$$

Octet and singlet free energies calculable at high T to LO in the Hard Thermal Loop approximation

$$\begin{aligned} F_1(r,T) &= -\frac{N^2-1}{2N}\frac{\alpha_s}{r}\exp(-m_D r) - \frac{(N^2-1)\alpha_s m_D}{2N} \\ F_8(r,T) &= \frac{1}{2N}\frac{\alpha_s}{r}\exp(-m_D r) - \frac{(N^2-1)\alpha_s m_D}{2N} \end{aligned}$$

Temperature dependence of $F(r,T)$ much stronger than for $F_1(r,T)$

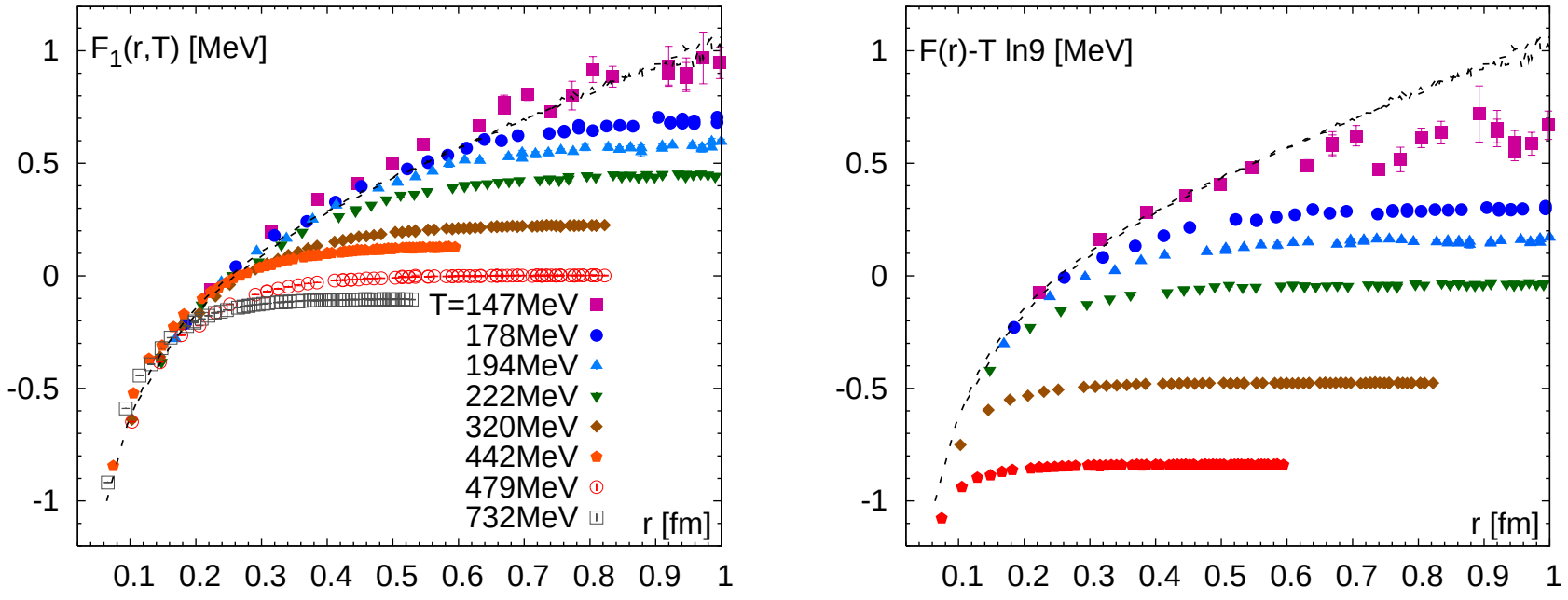

Figure 33: The singlet free energy as a function of the quark separation distance, r (left) and the free energy of a static $Q\overline{Q}$ pair (right). Both plots show the same temperature values. [arXiv:1302.2180]

Spectral Functions

In-medium properties encoded in spectral functions, σ, defined by Fourier transform of real-time two-point functions, $D^>$ and $D^<$, of meson current J_H

Current takes the form $J_H(t,x) = \bar{q}(t,\vec{x})\Gamma_H q(t,\vec{x})$ where $q(t,\vec{x})$ is quark field operator and $\Gamma_H = 1, \gamma_5, \gamma_\mu, \gamma_5\gamma_\mu, \gamma_\mu\gamma_\nu$ represent different quantum numbers

$$\begin{aligned}
\sigma(\omega,\vec{p}) &= \frac{1}{2\pi}(D_H^>(\omega,\vec{p}) - D_H^<(\omega,\vec{p})) = \frac{1}{\pi} Im D_H^R(\omega,\vec{p}) \\
D_H^{>(<)}(\omega,\vec{p}) &= \int_{-\infty}^{\infty} dt \int d^3x e^{i\omega t - i\vec{p}\cdot\vec{x}} D_H^{>(<)}(t,\vec{x}) \\
D_H^>(t,\vec{x}) &= \langle J_H(t,\vec{x}) J_H(0,\vec{0})\rangle \\
D_H^<(t,\vec{x}) &= \langle J_H(0,\vec{0}) J_H(t,\vec{x})\rangle, t > 0
\end{aligned}$$

Stable meson configuration is a delta function, $\sigma(\omega,\vec{p}) = |\langle 0|J_H|H\rangle|^2 \epsilon(\omega)\delta(p^2 - M^2)$

Table 3: Meson states in different channels for light, charm, and bottom quarks.

	Γ	$^{2S+1}L_J$	J^{PC}	$u\overline{u}$	$c\overline{c}(n=1)$	$c\overline{c}(n=2)$	$b\overline{b}(n=1)$	$b\overline{b}(n=2)$
PS	γ_5	$^1S_0$	0^{-+}	π	η_c	$\eta_c^{'}$	η_b	η_b'
V	γ_s	$^3S_1$	1^{--}	ρ	J/ψ	ψ'	$\Upsilon(1S)$	$\Upsilon(2S)$
T	$\gamma_s\gamma_{s'}$	$^1P_1$	1^{+-}	b_1	h_c		h_b	
S	1	$^3P_0$	0^{++}	a_0	χ_{c0}		$\chi_{b0}(1P)$	$\chi_{b0}(2P)$
AV	$\gamma_5\gamma_s$	$^3P_1$	1^{++}	a_1	χ_{c1}		$\chi_{b1}(1P)$	$\chi_{b1}(2P)$

In-medium there is a smeared peak with width equal to thermal width, when sufficiently broad, can't speak of a bound state

Spectral Functions Expressed Through Correlators

Integral representation of Euclidean time correlator

$$G(\tau,\vec{p}) = \int_0^\infty d\omega \sigma(\omega,\vec{p}) K(\omega,\tau) \ , \qquad K(\omega,\tau) = \frac{\cosh(\omega(\tau - 1/2T))}{\sinh(\omega/2T)}$$

Spectral functions divided into low ω part with narrow peak and high ω part in continuum which does not show a strong T dependence

Early attempts in pure glue theory involved the Maximum Entropy Method (MEM)

Found bound states surviving up to $\sim 2T_c$, different from results on color screening of F_1

Correlators are insensitive to spectral functions because the quarkonium state breaks up

New analysis shows there are no bound states in medium

Spatial correlators are more sensitive to in-medium modification

$$G(z,T) = \int_{-\infty}^{\infty} dp_z e^{ip_z z} \int_0^\infty d\omega \frac{\sigma(\omega,p_z,T)}{\omega}$$

Medium effects largest at $r > 1/T$ where $G(z,T)$ decays exponentially with screening mass $2\sqrt{(\pi T)^2 + m_Q^2}$ where πT is the lowest Matsubara frequency

Spectral Functions and Correlators

Real part of potential based on lattice free energy, all states but $\Upsilon(1S)$ vanish in QGP, large enhancements of spectral functions in the threshold region, no J/ψ bound state already at $T \sim 1.2T_c$

Only weak temperature dependence of correlators, explained because while the difference between vacuum and medium spectral functions grows, the Euclidean time extent, $1/(2T)$ decreases, making change hard to see – in addition, the threshold enhancements of the spectral functions compensates for the absence of bound states

These results are independent of the choice of potential as long as it is consistent with lattice

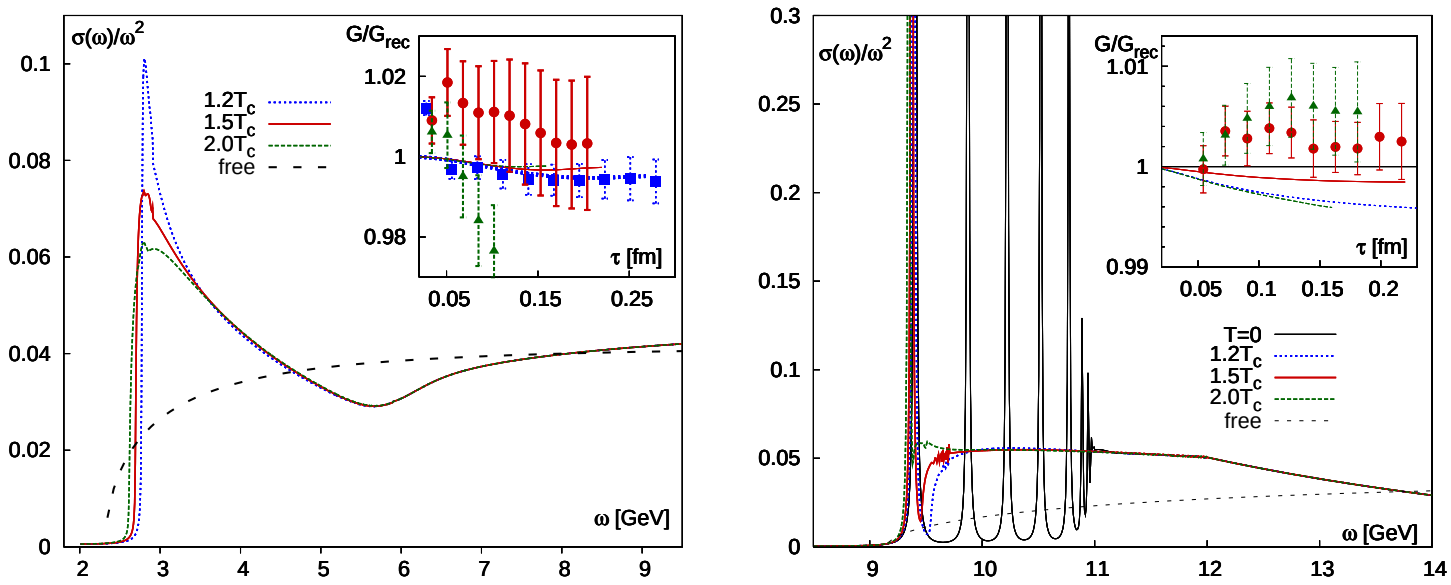

Figure 34: The S wave charmonium (left) and bottomonium (right) spectral functions calculated in quenched QCD using a lattice-inspired potential. The insets show the ratios of the correlators relative to the reconstructed correlator, $G_{\rm rec}$, compared to the lattice results. (The ratio $G/G_{\rm rec}$ should be unity if the spectral function is unchanged across the deconfinement transition.) [arXiv:1302.2180]

Effective Field Theories: Separation of Scales

At $T = 0$, velocity expansion: m_Q highest scale (NRQCD); $m_Q v \sim m_Q/r$ intermediate scale (pNRQCD), dynamical fields are singlet and octet $Q\overline{Q}$ states; $m_Q v^2 \sim \alpha_s/r$ lowest scale, dynamical fields are light quarks and gluons

Finite temperature, weak coupling, also has 3 separate scales: T, gT and g^2T. In the static limit (mv at $T = 0$), the binding energy (BE) is the difference between octet and singlet potentials, $V_o - V_s \simeq N\alpha_s/(2r)$

- **if BE $> T$, pNRQCD is derived the same way as at $T = 0$ and heavy quark potential is not modified by the medium**
- **This does not mean the bound states are unaffected by the medium – BE is reduced and the state acquires a finite thermal width**
- **If BE $< T$, V_o and V_s become T dependent and acquire an imaginary part: gluons exchanged in singlet-octet transitions scatter off thermal excitations in medium**
- **Thermal corrections to the potential come in as *e.g.* $(m_D r)^n$ (m_D is Debye mass)**
- **For $r > 1/m_D$ there is exponential screening and $V_s(r) = -(4\alpha_s/(3r))\exp(-m_D r) + i\mathcal{O}(\alpha_s)$ where the real part is the LO result for the free energy**
- **Imaginary part vanishes at short distance but is twice heavy quark damping rate at large distance**
- **As T increases, BE$\rightarrow 0$ and medium effects are incorporated into potential, separation of thermal scales fails and lattice results required to constrain potential**

Point of Zero Binding

If real part of BE is positive, state is bound, dissociation temperature defined as when the real and imaginary parts of BE are equal

Note that the precise value of the dissociation temperature is not all that important because the state is undergoing in-medium decays even below this value

Imaginary part gives information about decay rate, $n(t) = n_0 \exp(-\Gamma(\tau - \tau_0))$ so that the decay rate, Γ, is -2 times the imaginary part

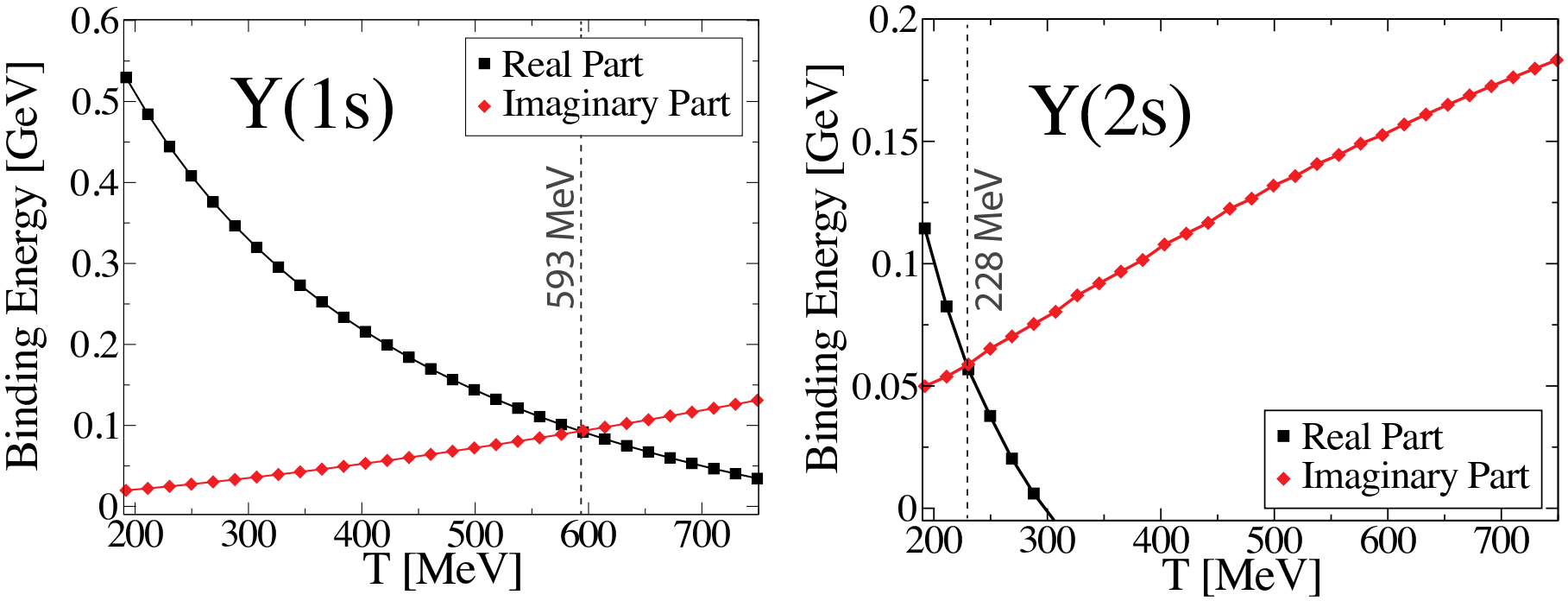

Figure 35: Real and imaginary parts of the binding energy for $\Upsilon(1S)$ (left) and $\Upsilon(2S)$ (right) as a function of temperature for an isotropic QGP. [arXiv:1302.2180]

Systems Away From Thermal Equilibrium

Typical viscous hydrodynamical calculations assume system is close to thermal equilibrium and thus also isotropic in momentum space

However, large initial momentum anisotropies can persist throughout the lifetime of the plasma

For quarkonium, this is accounted for by introducing anisotropy parameter ξ, related to the ellipticity of momentum distribution $(p_T - p_L)$

Primary effect of anisotropy is reduction of Debye screening, leading to higher dissociation temperatures

	T_D (MeV)	
State	Isotropic QGP (ξ=0)	Anisotropic QGP (ξ=1)
J/ψ	307	374
χ_{c1}	< 192	210
$\Upsilon(1S)$	593	735
$\Upsilon(2S)$	228	290
$\Upsilon(3S)$	< 192	< 192
χ_{b1}	265	351
χ_{b2}	< 192	213

Table 4: Estimates of the isotropic and anisotropic dissociation scales for the J/ψ, χ_{c1}, $\Upsilon(1S)$, $\Upsilon(2S)$, $\Upsilon(3S)$, χ_{b1}, and χ_{b2}. [arXiv:1302.2180]

Effects of Anisotropic Plasma on Υ Production

Screening mass taken to depend on plasma anisotropy, $\mu = G(\xi, \theta) m_D$ where θ is angle of the line between the $Q\overline{Q}$ and the beam direction

Viscous hydro calculation with $\tau_0 = 0.3$ fm, $T_0 = 500$ MeV (to fit $dN_{\rm ch}/d\eta \sim 1400$), find what value of $4\pi\eta/S$ agrees best with CMS Υ data as a function of $N_{\rm part}$

Best agreement is with $4\pi\eta/S = 3$ (consistent with IP-Sat flow results, $\eta/S = 0.2$ ($4\pi\eta/S \sim 2.5$)

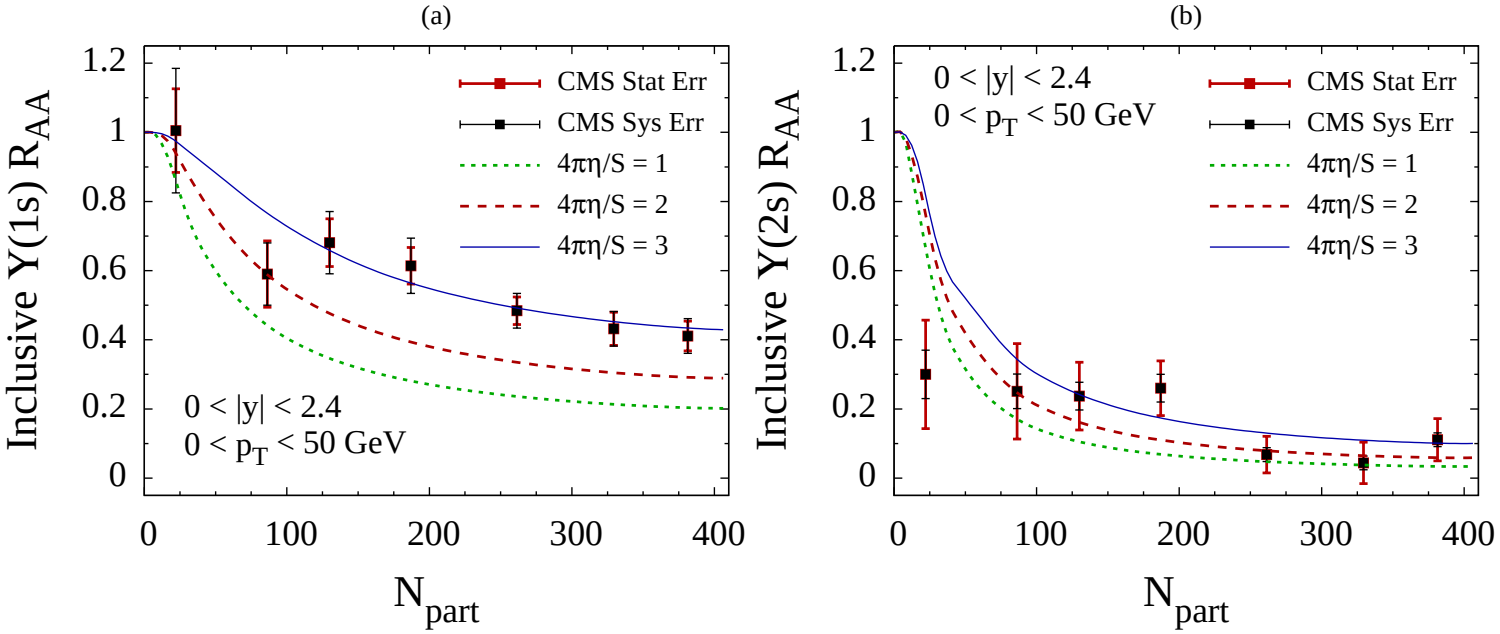

Figure 36: (Top) Real and imaginary parts of the binding energy for $\Upsilon(1S)$ (left) and $\Upsilon(2S)$ (right) as a function of temperature for an isotropic QGP. [arXiv:1302.2180] (Bottom) Suppression factor R_{AA} as a function of $N_{\rm part}$ for several values of the viscosity to entropy ratio compared to preliminary CMS data [M. Strickland, arXiv:1207.5327].

Excited States

J/ψ vs. ψ'

J/ψ is smaller and more tightly bound than the ψ' so ψ' is easier to break up in interactions with nucleons and comoving hadrons

The ψ' has a lower dissociation temperature

ψ' has no feed down, only direct (and non-prompt) production [inclusive = prompt + non-prompt]

Non-prompt decays more important for ψ' since the branching for $B \to \psi' X$ is larger than for $B \to J/\psi X$

Chen *et al.* (arXiv:1306.5032) used Boltzmann transport equation to calculate the phase space distributions of charmonia including a loss term, $-\alpha_C$, due to in-medium suppression and a gain term, β_C, from recombination (C is the charmonium state)

$$\frac{\partial \overline{f}_C}{\partial t} + \vec{v} \cdot \nabla \overline{f}_C = -\alpha_C \overline{f}_C + \beta_C$$

The phase space distribution at the hadronization time is used to compute the charmonium distributions and thus the suppression factors R_{AA} for J/ψ and ψ'

The inclusive nuclear suppression factor contains the prompt contribution, $R^C_{AA} = \overline{N}^C_{AA}/(N_{\rm bin}\overline{N}^C_{pp})$, and the ratio of non-prompt to prompt production, $r^C_B = N^{B\to C}_{pp}/\overline{N}^C_{pp}$, modified by the b quark energy loss, Q

$$R^C_{AA} = \frac{\overline{R}^C_{AA} + r^C_B Q}{1 + r^C_B}$$

Comparison to ψ'/ψ Double Ratio

Difficult to compare data sets, all at different rapidities with different p_T ranges, CMS forward ratio suffers from low pp statistics

Kinks in calculations correspond to N_p where T is J/ψ dissociation temperature, none of the calculations give a double ratio greater than unity

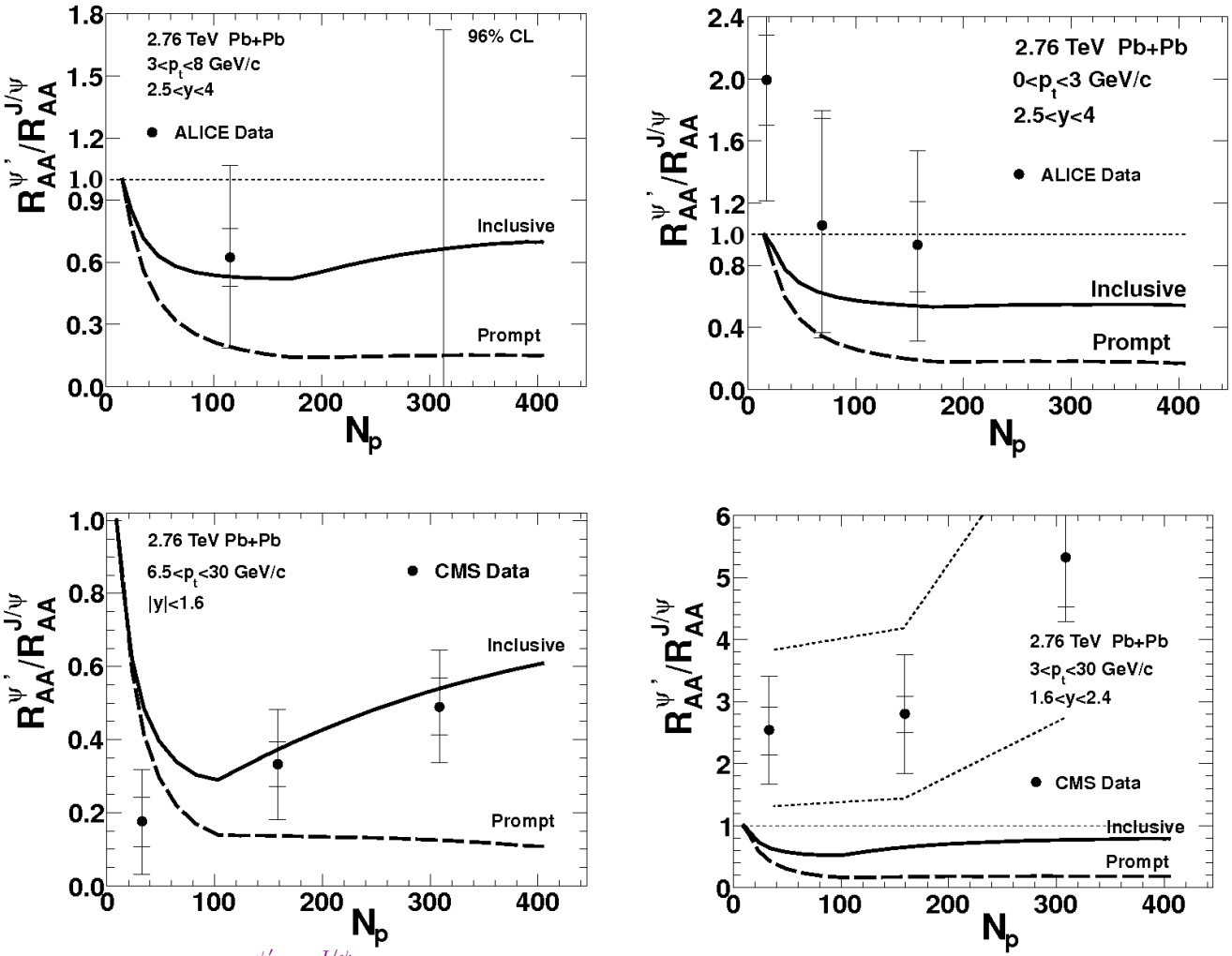

Figure 37: All plots show the double ratio $R_{AA}^{\psi'}/R_{AA}^{J/\psi}$ as a function of the number of participants $N_{\rm part} \equiv N_p$. The lines labeled 'inclusive' include B decays while those labeled 'prompt' do not. (Top) ALICE forward data $2.5 < y < 4$ at low, $p_T < 3$ GeV (left) and intermediate, $3 < p_T < 8$ GeV, p_T (right). (Bottom left) CMS central data, $|y| < 1.6$, for $6.5 < p_T < 30$ GeV. (Bottom right) CMS more forward data, $1.6 < |y| < 2.4$, $3 < p_T < 30$ GeV.

Open Heavy Flavor

Heavy Quark Diffusion and Drag

Heavy quark dynamics in medium described by relativistic Langevin equation with drag coefficient, $\eta_D(p)$ describing the friction of the medium and diffusion coefficient $\vec{\xi}(t)$ accounting for collisions with medium constituents

$$\frac{\Delta\vec{p}}{\Delta t} = -\eta_D(p)\vec{p} + \vec{\xi}(t)$$

Expectation value $\langle \xi^i(t)\xi^j(t')\rangle$ related to tensor decomposed as

$$\kappa_L(p)\hat{p}^i\hat{p}^j + \kappa_T(p)(\delta^{ij} - \hat{p}^i\hat{p}^j)$$

Transport coefficients $\kappa_{L,T}(p)$ represent the squared longitudinal/transverse momentum per unit time exchanged with the medium

$\eta_D(p)$ fixed so that at large time, the momenta of an ensemble of heavy quarks approaches a thermal distribution

$$\eta_D(p) = \frac{\kappa_L(p)}{2TE}$$

In Alberico *et al* [arXiv:1305.7421], $\kappa_{L,T}$ include soft part, obtained in either the hard thermal loop approximation or directly from lattice QCD, and a perturbatively calculable hard part

In He *et al* [arXiv:1106.6006], the drag coefficient $\eta_D(p)$ is related to heavy quark relaxation rate and is calculated using in-medium heavy-light quark T-matrices via resonant rescattering, includes recombination

Model Comparison of Non-photonic R_{AA} and v_2 at RHIC

Alberico lattice transport coefficients give a stronger p_T dependence (weaker R_{AA} at high p_T) than the HTL result, neither agrees well with data; little flow generated

He's agreement is better at low p_T, perhaps due to recombination, more flow generated

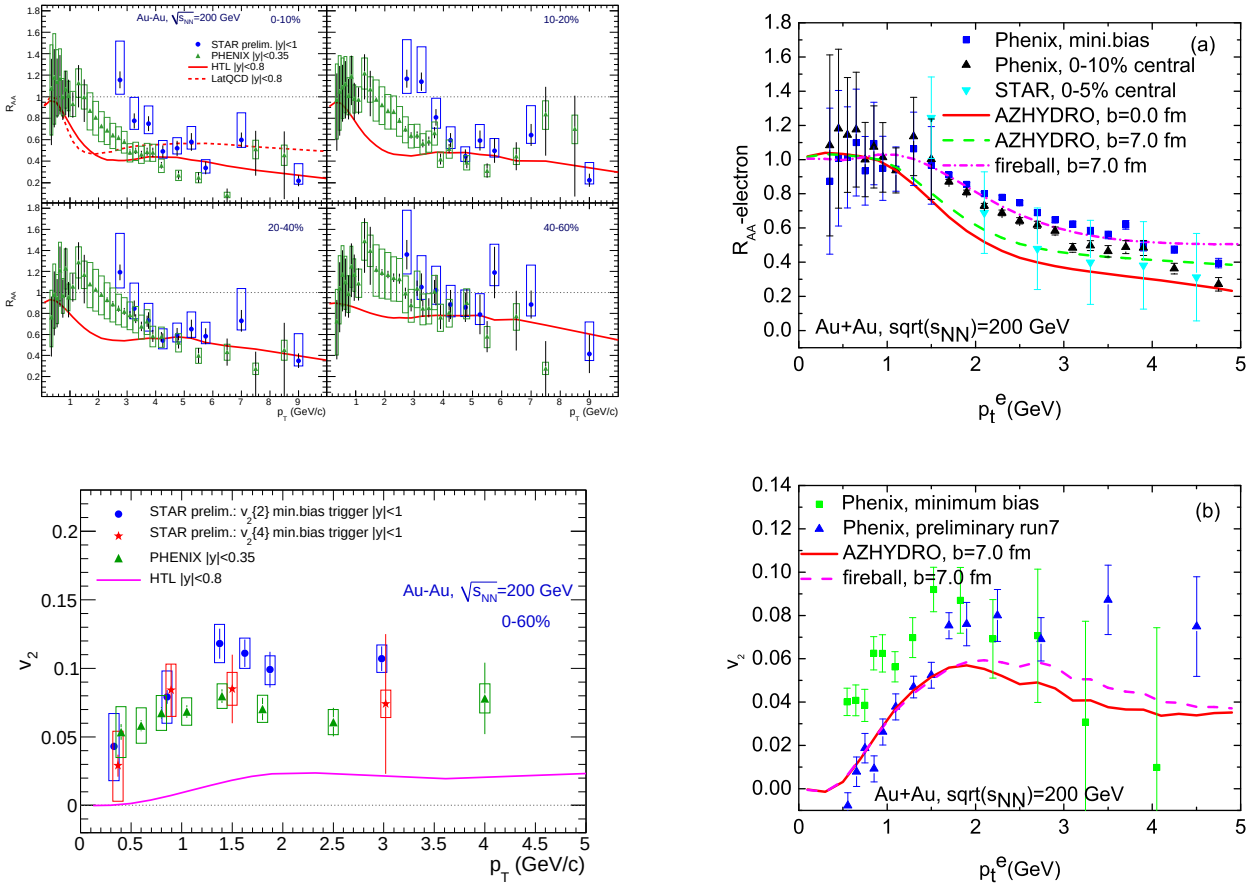

Figure 38: (Top) Non-photonic electron R_{AA} results from RHIC compared to Langevin calculations by Alberico *et al.* [arXiv:1305.7421] (left) and He *et al.* [arXiv:1106.6006] (right). (Bottom) Non-photonic electron v_2 results from RHIC compared to Langevin calculations by Alberico *et al.* [arXiv:1305.7421] (left) and He *et al.* [arXiv:1106.6006] (right).

b-jet Quenching

b quarks produced in PYTHIA via 3 mechanisms: standard LO production (R_b); gluon splitting ($R_{\rm gluon}$); and other LO jet production processes, *e.g.* $q\overline{q} \to q\overline{q}$ ($R_{\rm other}$)

Contribution from gluon splitting decreases if b-quark is leading particle in the jet

Results depend on cone size (larger cone radius reduces suppression), inclusion of collisional dissipation (increases suppression), in-medium coupling (larger coupling increases suppression) and mass of propagating parton (widens uncertainty at $p_T <$ 75 GeV) – CNM effects are small

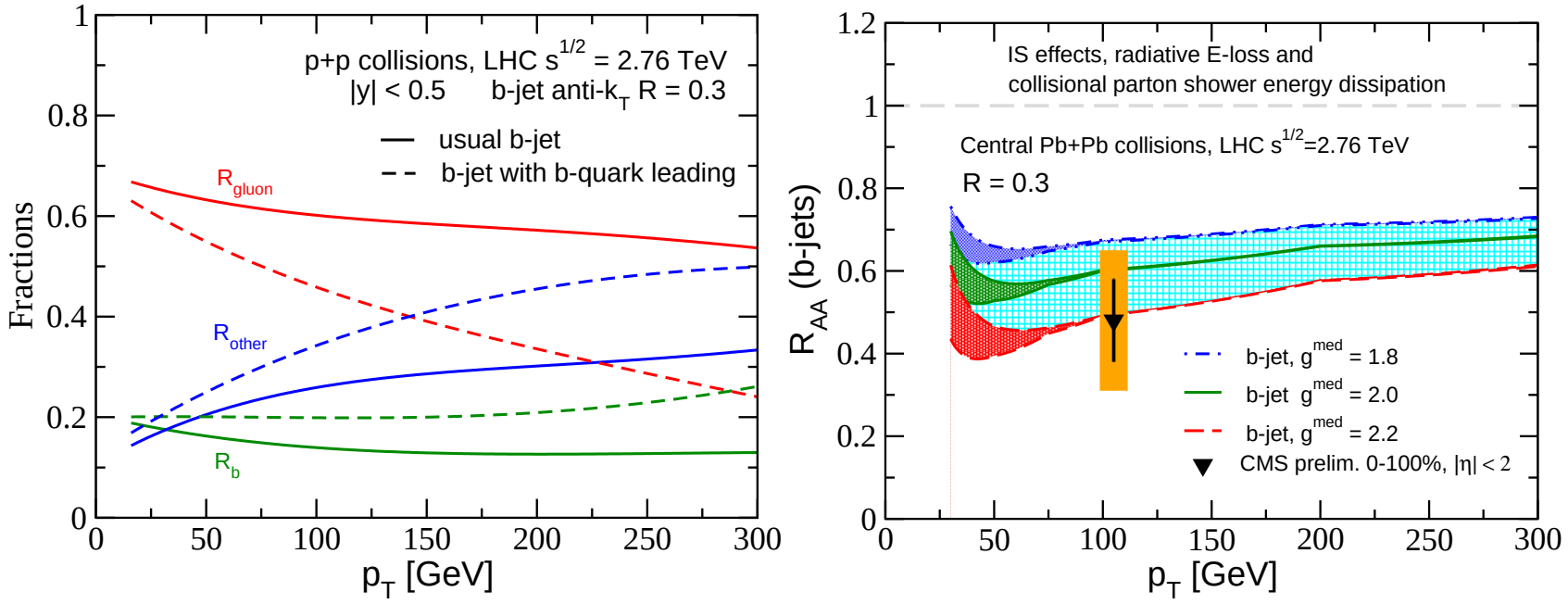

Figure 39: (Left) Relative contributions to inclusive b-jet production in PYTHIA8. The solid curves show the results for conventional jet production while the dashed curves require that the b quark be the leading particle in the jet. (Right) The b-jet suppression for three different in-medium couplings with $|\eta| < 2$, anti-k_T jet algorithm with $R = 0.3$, including CNM effects as well as collisional and radiative energy loss. [Huang *et al.*, arXiv:1306.0909.]

One Last Thought

How Do We Define Suppression? (Satz)

Quarkonium and open heavy flavor are generally considered as two completely different entities even though they share most of the same cold matter effects (in particular shadowing and energy loss)

We saw before that the A dependence of J/ψ and open charm are similar away from midrapidity (fixed target E866 data); difference at midrapidity could perhaps be attributed to absorption-like effects

However, in AA collisions, if R_{AA} is the same for J/ψ and D mesons, is it *really* J/ψ suppression?

Use open charm production as a baseline for J/ψ suppression

Let the number of $c\overline{c}$ pairs that form a J/ψ in pp collisions be defined as $g_{c\overline{c}\to J/\psi} = N_{pp}(J/\psi)/N_{pp}(c\overline{c})$

For $R_{AA}(J/\psi) = N_{AA}(J/\psi)/(N_{\rm bin}N_{pp}(J/\psi)$ and $R_{AA}(c\overline{c}) = N_{AA}(c\overline{c})/(N_{\rm bin}N_{pp}(c\overline{c})$, the true J/ψ survival probability is

$$S_{J/\psi} = \frac{N_{AA}(J/\psi)/N_{AA}(c\overline{c})}{N_{pp}(J/\psi)/N_{pp}(c\overline{c})} = \frac{R_{AA}(J/\psi)}{R_{AA}(c\overline{c})} = \frac{1}{g_{c\overline{c}\to J/\psi}}\frac{N_{AA}(J/\psi)}{N_{AA}(c\overline{c})}$$

If $R_{AA}(J/\psi) = R_{AA}(c\overline{c})$, then $S_{J/\psi} \equiv 1$

Is J/ψ Suppressed Relative to Open Charm? Intermediate and High p_T at the LHC Says No

Comparison of ALICE and CMS J/ψ and D meson data at $\sqrt{s_{NN}} = 2.76$ TeV.

ALICE results on left, D mesons at midrapidity, J/ψ at forward, $p_T \neq 0$ for both CMS and ALICE measurements both at midrapidity although CMS covers larger range and goes to higher p_T

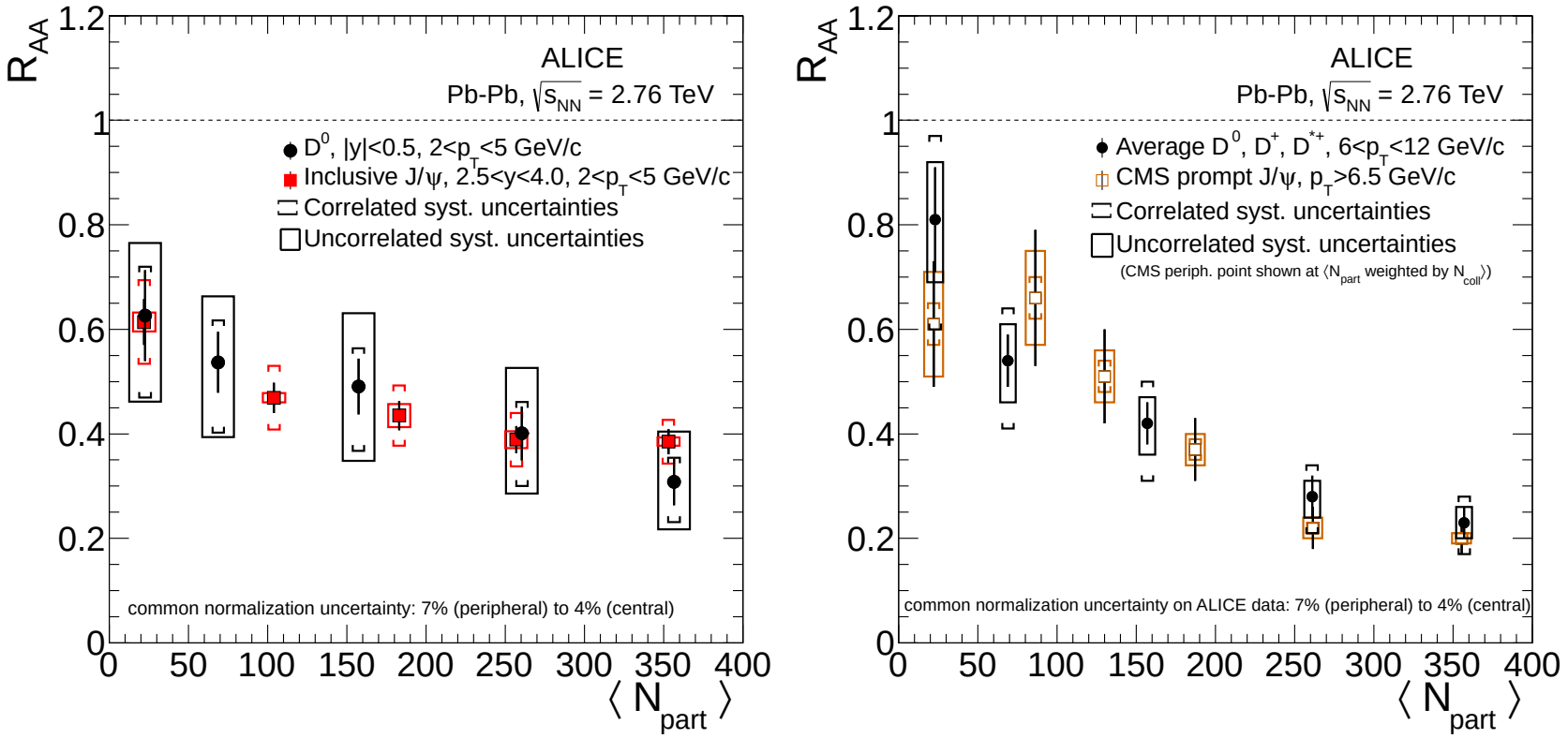

Figure 40: Comparison of ALICE midrapidity D mesons and forward J/ψ at intermediate p_T (left) and of ALICE D mesons and CMS J/ψ at midrapidity for higher p_T (right). [Satz, arXiv:1303.3493.]

Is J/ψ Suppressed Relative to Open Charm? Low p_T at RHIC Says Yes, Higher p_T, Maybe Not

The "$D \to e$" result shows different behavior from the J/ψ at low p_T but NB, the "D" decays are non-photonic electrons, some B decay mixing, small at low p_T

We thus need to be careful about how we define J/ψ suppression

'Real' J/ψ suppression only at low p_T and, after Debye screening ends same mechanism for open and closed heavy flavor suppression?

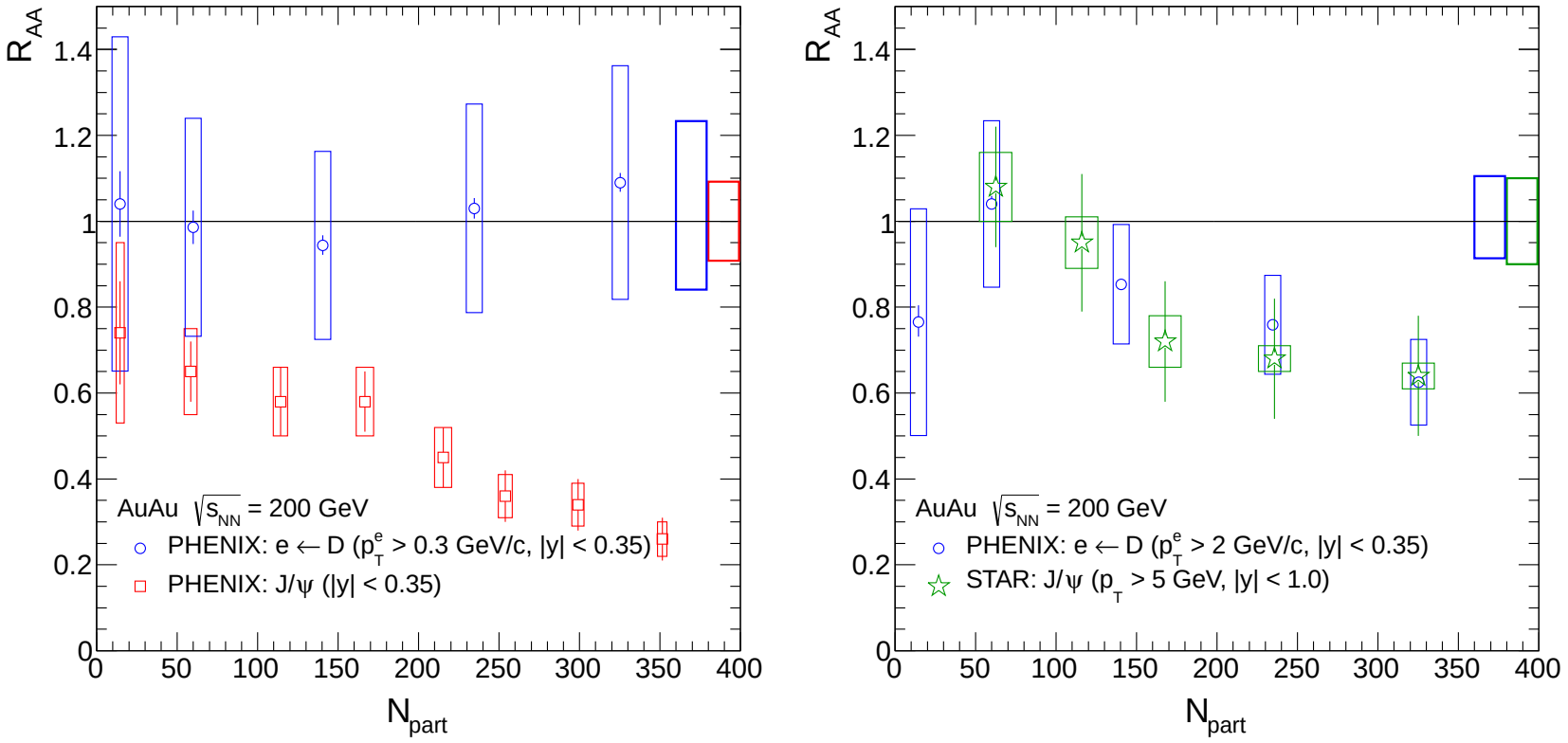

Figure 41: Comparison of PHENIX $D \to e$ decays J/ψ at midrapidity at low p_T (left) and PHENIX $D \to e$ decays and STAR J/ψ at high p_T (right). [Satz, arXiv:1303.3493.]

Summary of AA

- **Cold matter effects insufficient to explain AA data but ultraperipheral collisions may allow a cleaner measure of gluon shadowing**
- **Lattice calculations of spectral functions have evolved to be more precise and predictive**
- **Imaginary part of the potential tells us that the state decays in the medium so that dissociation occurs even below T_D**
- **Ratios of excited to ground states could help distinguish between models if data are improved**
- **Including hadronization of D mesons by recombination produces more consistent results for R_{AA} and v_2 than without**
- **We should consider whether J/ψ is really suppressed if $R_{AA}(J/\psi) = R_{AA}(c\overline{c})$: Effective QGP suppression from $p_T \sim 0$ to only few GeV (where regeneration may also play a role) while at higher p_T energy loss may dominate for J/ψ**

Thanks to the Organizers.